

RIS-aided Zero-Forcing and Regularized Zero-Forcing Beamforming in Integrated Information and Energy Delivery

H. Yu¹, H. D. Tuan¹, E. Dutkiewicz¹, H. V. Poor², and L. Hanzo³

Abstract—This paper considers a network of a multi-antenna array base station (BS) and a reconfigurable intelligent surface (RIS) to deliver both information to information users (IUs) and power to energy users (EUs). The RIS links the connection between the IUs and the BS as there is no direct path between the former and the latter. The EUs are located nearby the BS in order to effectively harvest energy from the high-power signal from the BS, while the much weaker signal reflected from the RIS hardly contributes to the EUs' harvested energy. To provide reliable links for all users over the same time-slot, we adopt the transmit time-switching (transmit-TS) approach, under which information and energy are delivered over different time-slot fractions. This allows us to rely on conjugate beamforming for energy links and zero-forcing/regularized zero-forcing beamforming (ZFB/RZFB) and on the programmable reflecting coefficients (PRCs) of the RIS for information links. We show that ZFB/RZFB and PRCs can be still separately optimized in their joint design, where PRC optimization is based on iterative closed-form expressions. We then develop a path-following algorithm for solving our maxim IU throughput optimization problem subject to a realistic constraint on the quality-of-energy-service in terms of the EUs' harvested energy thresholds. We also propose a new RZFB for substantially improving the IUs' throughput.

Index Terms—Reconfigurable intelligent surface, transmit beamforming, conjugate beamforming, zero-forcing beamforming, trigonometric function optimization, concave optimization.

I. INTRODUCTION

Jointly supporting both wireless information and power transfer networking poses challenging problems in signal processing for communication (see e.g. [1] and references therein). For information and energy delivery over a single time slot, simultaneous wireless information and power transfer (SWIPT) apportions the power of the signals received by the users for energy-harvesting (EH) and information detection (ID). In the context, the EH performance is dependent on the power of the received signal, by contrast, the ID performance is critically dependent on the signal-to-interference-plus-noise ratio (SINR). The popular SWIPT systems have primarily

used conjugate beamforming (CB) to deliver sufficient energy for EH [2], even though this limits the ID performance due to the multi-user interference (MUI) imposed. By contrast, zero-forcing beamforming (ZFB) completely eliminates the MUI, but it is less efficient for SWIPT. To circumvent these drawbacks, it has been proposed to convey information and energy over the same time slot by transmitting information and energy in separate fractions of the time-slot. Termed as transmit time-switching (transmit-TS), it has been shown to outperform SWIPT due to its ability to support individual energy beamforming for EH and information beamforming for ID (see e.g. [3]–[6]). As a benefit, transmit-TS enables CB for EH and ZFB or regularized zero-forcing beamforming (RZFB) for ID [7], [8] [6].

A reconfigurable intelligent surface (RIS) is a planar array of "nearly-passive" reflecting elements, which can beneficially manipulate the reflected signals by programming its reflection coefficients [9]. By strategically installing a RIS in places such as building facades so that it can have a line-of-sight (LoS) path from both the users and a base station (BS), the RIS facilitates reliable communication when there are no direct links between them [10]–[13]. A challenging problem in signal processing for these RIS-aided networks is to jointly design the BS's transmit beamformers and the RIS's programmable reflecting coefficients (PRCs) to maximizing the sum throughput [10], [14]–[16] or the users' minimum throughput [17]. The joint design of power allocation for ZFB and PRCs to maximize the sum throughput subject to individual user throughput constraints has been considered in [10]. While the alternating power allocation optimization with the PRCs held fixed is simple, the alternating optimization in PRCs with the power allocation held fixed is very challenging since the user throughput becomes a complex function due to the matrix inversion involved in ZFB. As a result, the convergence behavior of the general purpose gradient descent algorithm used in [10] is unknown. Thus, the expected computational tractability of the ZFB design could not be achieved. The authors of [18] and [19] considered some RIS-aided SWIPT scenarios which require that the BS, the RIS and the energy users (EUs) must be located within a small cell radius of about 10m, however the reflected signal by the RIS after undergoing the associated double path-loss becomes quite weak compared to that coming directly from the BS to the EUs, which erodes the benefit of the RIS in EH.

Against the above background, this paper offers the following contributions.

This work was supported in part by the Australian Research Councils Discovery Projects under Grant DP190102501, and in part by the Engineering and Physical Sciences Research Council projects EP/P034284/1 and EP/P003990/1 (COALESCE), and European Research Council's Advanced Fellow Grant QuantCom (Grant No. 789028)

¹School of Electrical and Data Engineering, University of Technology Sydney, Broadway, NSW 2007, Australia (email: Hongwen.Yu@student.uts.edu.au, Tuan.Hoang@uts.edu.au, Eryk.Dutkiewicz@uts.edu.au); ²Department of Electrical and Computer Engineering, Princeton University, Princeton, NJ 08544, USA (email: poor@princeton.edu); ³School of Electronics and Computer Science, University of Southampton, Southampton, SO17 1BJ, UK (email: lh@ecs.soton.ac.uk)

- We reveal that as a benefit of the transmit-TS technique, the joint optimization of power allocations (for ZFB) and PRCs may be simplified to optimizing the PRCs only, because the power allocation for ZFB can be easily determined. Instead of iterating by relying on convex problems or using deep Q-learning methods to handle the unit-modulus constraint on the PRCs which incur much higher computational complexity [17], [20], [21], we use the polar form of unit-modulus complex numbers that allows each descent iteration of the RIS coefficient calculation to be based on computational efficient closed-form expressions for the solution of concave trigonometric function optimization [22]. Accordingly, we develop efficient computational procedures, which are based on closed-form expressions for its computation;
- Similarly, we also show that the joint optimization of power allocations (for RZFB) and PRCs can be decomposed into the separate optimization of power allocations (for RZFB) and optimization of PRCs. Accordingly, we develop efficient computational procedures for PRC optimization, which are still based on closed-form expressions. A computational procedure is also proposed for power allocations optimization, which involves a convex quadratic problem at each iteration;
- Furthermore, we develop a new RZFB for improving the throughput of IUs. Our simulations show that the IUs' throughput using the new RZFB is 15% - 25% higher than that obtained by the existing RZFB in the challenging rank-deficient scenario, when the BS only has a few antennas for serving more IUs;
- We consider a practical scenario of RIS-aided integrated information and energy deliveries to both information users (IUs) and energy users (EUs). By adopting the aforementioned transmit-TS approach, we harness CB for delivering energy to EUs, and RIS-aided ZFB/RZFB/new RZFB for delivering information to IUs. Naturally, the PRCs are still separately optimized in this joint design problem. We then develop efficient computational procedures for solving the problem of maximizing the IUs' minimum throughput subject to a constraint on the quality-of-energy-service (QoES) in terms of the EUs' harvested energy thresholds.

The rest of the paper is organized as follows. Section II and Section III are respectively devoted to PRC optimization for ZFB and RZFB with its applications to RIS-aided information and energy delivery studied in Section IV and V. A new RZFB is also introduced in Section V. Section VI provides simulations to support the technical developments of the previous sections. Section VII concludes the paper. The Appendix provides several inequalities that are frequently used in the technical sections. The flow chart of paper organization can be seen in Fig. 1.

Notation. Only design variables are denoted in bold face; $\mathcal{C}(0, a)$ is the set of circular Gaussian random variables with zero means and variances a ; $\angle x_i$ is the argument of the complex number x_i and as such $\angle x$ for $x = (x_1, \dots, x_N)^T \in \mathbb{C}^N$ is understood componentwise: $\angle x \triangleq (\angle x_1, \dots, \angle x_N)^T \in$

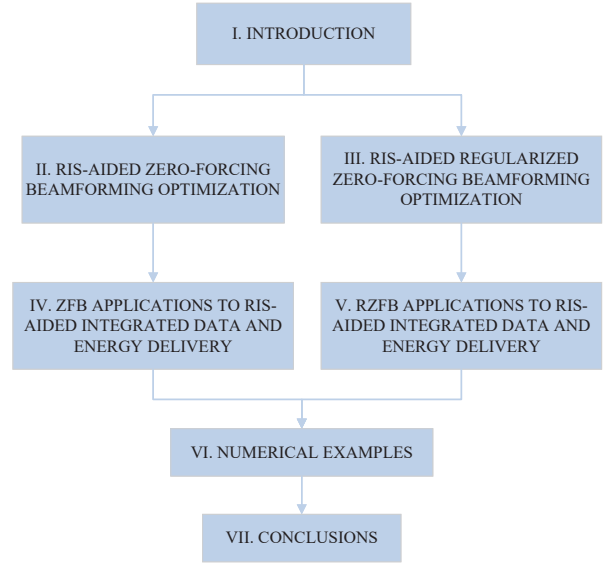


Fig. 1: Paper organization.

\mathbb{C}^N ; I_N is the identity matrix of size $N \times N$, while $O_{M \times N}$ is a zero matrix of size $M \times N$; for $x = (x_1, \dots, x_N)^T$, $\text{diag}(x)$ is a diagonal matrix of size $N \times N$ with x_1, x_2, \dots, x_N on its diagonal; we also write $\langle X \rangle = \text{trace}(X)$ for notational simplicity; $[X]^2$ is XX^H , so $[X^H]^2 = X^H X$, and $\langle X, Y \rangle = \langle X^H Y \rangle$ for matrices X and Y ; accordingly, the Frobenius norm of X is defined by $\|X\| = \sqrt{\langle [X]^2 \rangle}$; the notation $X \succeq 0$ ($X \succ 0$, resp.) used for the Hermitian symmetric matrix X indicates that it is positive definite (positive semi-definite, resp.); the maximal eigenvalue of the Hermitian symmetric matrix X is denoted by $\lambda_{\max}(X)$.

II. RIS-AIDED ZERO-FORCING BEAMFORMING OPTIMIZATION

Consider a RIS-aided network, which is illustrated by Fig. 2 with a RIS of N reflecting units to assist the downlink from an M -antenna base station (BS) to K single-antenna information users (IUs) $k \in \mathcal{K} \triangleq \{1, \dots, K\}$ because there is no direct signal path between the former and the latter.¹ The channel spanning from the BS to the RIS is $\tilde{H}_{B-R} \triangleq \sqrt{\beta_{B-R}} H_{B-R} \in \mathbb{C}^{N \times M}$, where $\sqrt{\beta_{B-R}}$ models the path-loss and large-scale fading of LoS and the entries of H_{B-R} are $\mathcal{C}(0, 1)$, modelling small-scale fading. Analogously, the channel spanning from the RIS to IU k is $\tilde{h}_{R-k} = \sqrt{\beta_{R-k}} \bar{h}_{R-k} \in \mathbb{C}^{1 \times N}$, where $\sqrt{\beta_{R-k}}$ represents the large-scale fading, while \bar{h}_{R-k} denotes the small-scale fading having elements of $\mathcal{C}(0, 1)$. Like in many other papers on RIS-aided communication networks, we assume perfect channel state information, which can be obtained by channel estimation [19], [20], [24].

Let $\boldsymbol{\theta} \triangleq (\boldsymbol{\theta}_1, \dots, \boldsymbol{\theta}_N) \in [0, 2\pi]^N$ and

$$e^{j\boldsymbol{\theta}} \triangleq (e^{j\boldsymbol{\theta}_1}, \dots, e^{j\boldsymbol{\theta}_N})^T \in \mathbb{C}^N,$$

¹According to [17], [23], the networks throughput is hardly improved by RIS's, when there are direct paths from the BS to the IUs.

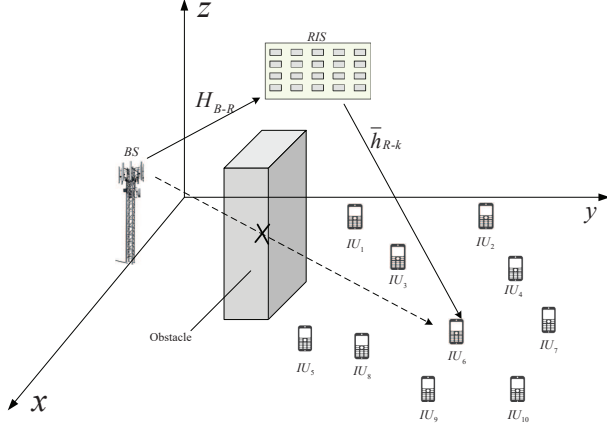


Fig. 2: Scenario setup with the blockage of the direct path between the BS and the IUs.

which is a complex-vector function of the variable θ . We also define the diagonal complex-matrix function of the variable $e^{j\theta}$ as

$$\text{diag}[e^{j\theta}] = \text{diag}\{e^{j\theta_1}, \dots, e^{j\theta_N}\} \in \mathbb{C}^{N \times N}$$

representing the matrix of RIS reflection-coefficients.

The received signal at IU k is

$$y_k = h_{B-k}(e^{j\theta})x_I + n_k, \quad (1)$$

where $n_k \in \mathcal{C}(0, \sigma)$ is the background noise, and

$$h_{B-k}(\theta) \triangleq \tilde{h}_{R-k} R_{RIS-k}^{1/2} \text{diag}[e^{j\theta}] \tilde{H}_{B-R} \in \mathbb{C}^{1 \times M}, \quad (2)$$

which is the composite channel spanning from the BS to IU k .

In (2), $R_{RIS-k} \in \mathbb{C}^{N \times N}$ represents the spatial correlation matrix of the RIS elements with respect to IU k [14]. For

$$y \triangleq \begin{bmatrix} y_1 \\ \dots \\ y_K \end{bmatrix} \in \mathbb{C}^K, \bar{n} \triangleq \begin{bmatrix} n_1 \\ \dots \\ n_K \end{bmatrix} \in \mathbb{C}^K,$$

and

$$\begin{aligned} \mathcal{H}(e^{j\theta}) &\triangleq \begin{bmatrix} h_{B-1}(e^{j\theta}) \\ \dots \\ h_{B-K}(e^{j\theta}) \end{bmatrix} = H_R \text{diag}[e^{j\theta}] \tilde{H}_{B-R} \\ &= \sum_{n=1}^N e^{j\theta_n} \mathcal{H}_n \in \mathbb{C}^{K \times M} \end{aligned}$$

with

$$\mathcal{H}_n \triangleq H_R \Psi_n \tilde{H}_{B-R} \in \mathbb{C}^{K \times M}$$

$$H_R \triangleq \begin{bmatrix} \tilde{h}_{R-1} R_{RIS-1}^{1/2} \\ \dots \\ \tilde{h}_{R-K} R_{RIS-K}^{1/2} \end{bmatrix} \in \mathbb{C}^{K \times N},$$

where Ψ_n is a matrix of size $N \times N$ with all-zero entries, excepts $\Psi_n(n, n) = 1$.

We can write

$$y = \mathcal{H}(e^{j\theta})x_I + \bar{n}. \quad (3)$$

Now, for $K \leq M$ we consider the ZFB, under which the BS transmits

$$x_I = \mathcal{H}^H(e^{j\theta}) \left([\mathcal{H}(e^{j\theta})]^2 \right)^{-1} \text{diag}[\mathbf{p}_k]_{k=1, \dots, K} s, \quad (4)$$

where $s = (s_1, \dots, s_K)^T$, $s_k \in \mathcal{C}(0, 1)$ is the information intended for the IUs having the power of $\mathbf{p} = (\mathbf{p}_1, \dots, \mathbf{p}_K)^T$. Then Equation (3) becomes

$$\begin{aligned} y &= \mathcal{H}(e^{j\theta}) \mathcal{H}^H(e^{j\theta}) \left([\mathcal{H}(e^{j\theta})]^2 \right)^{-1} \text{diag}[\mathbf{p}_k]_{k=1, \dots, K} s + \bar{n} \\ &= [\mathcal{H}(e^{j\theta})]^2 \left([\mathcal{H}(e^{j\theta})]^2 \right)^{-1} \text{diag}[\mathbf{p}_k]_{k=1, \dots, K} s + \bar{n} \\ &= \text{diag}[\mathbf{p}_k]_{k=1, \dots, K} s + \bar{n} \end{aligned} \quad (5)$$

simplifying (1) to

$$y_k = \mathbf{p}_k s_k + \bar{n}_k. \quad (6)$$

The throughput for s_k is

$$\ln(1 + \mathbf{p}_k^2 / \sigma), \quad (7)$$

and the transmit power is

$$\begin{aligned} \mathbb{E}(\|x_I\|^2) &= \langle \mathcal{H}^H(e^{j\theta}) \left([\mathcal{H}(e^{j\theta})]^2 \right)^{-1} \text{diag}[\mathbf{p}_k^2]_{k=1, \dots, K} \\ &\quad \left([\mathcal{H}(e^{j\theta})]^2 \right)^{-1} \mathcal{H}(e^{j\theta}) \rangle \end{aligned} \quad (8)$$

$$= \langle \text{diag}[\mathbf{p}_k^2]_{k=1, \dots, K} \left([\mathcal{H}(e^{j\theta})]^2 \right)^{-1} \rangle. \quad (9)$$

For the IUs' max-min throughput optimization is employed, which aims for maximizing the users' worst-case (minimal) throughput, where we have $\mathbf{p}_k \equiv \mathbf{p}_0^2 (\ln(1 + \mathbf{p}_k^2 / \sigma) \equiv \ln(1 + \mathbf{p}_0^2 / \sigma))$. Then by (9), the transmit power is $\mathbf{p}_0^2 \langle ([\mathcal{H}(e^{j\theta})]^2)^{-1} \rangle$, and the problem of max-min IU throughput optimization subject to a transmit power budget P can be formulated as

$$\max_{\mathbf{p}_0, \theta} \ln(1 + \mathbf{p}_0^2 / \sigma) \quad \text{s.t.} \quad \mathbf{p}_0^2 \langle ([\mathcal{H}(e^{j\theta})]^2)^{-1} \rangle \leq P \quad (10)$$

$$\Leftrightarrow \max_{\theta} P / \langle ([\mathcal{H}(e^{j\theta})]^2)^{-1} \rangle \quad (11)$$

$$\Leftrightarrow \min_{\theta} f(e^{j\theta}) \triangleq \langle (\mathcal{H}(e^{j\theta}) \mathcal{H}^H(e^{j\theta}))^{-1} \rangle. \quad (12)$$

In fact, it follows from the power constraint in (10) that $\mathbf{p}_0^2 \leq P / \langle ([\mathcal{H}(e^{j\theta})]^2)^{-1} \rangle$. Hence the problem (10) is actually $\max \ln(1 + P / (\sigma \langle ([\mathcal{H}(e^{j\theta})]^2)^{-1} \rangle))$, which is the same as (11). Since only the denominator of the fractional objective function in (11) is dependent on θ , its maximization is equivalent to the minimization of its denominator, which is (12).

The rest of this section is devoted to the detailed portrayal of our algorithms conceived for computing (12), which is very challenging because its objective function is highly nonlinear and computationally intractable.

²From (7), the users' worst-case throughput is $\min_{k=1, \dots, K} \ln(1 + \mathbf{p}_k^2 / \sigma)$, which is maximized at $\ln(1 + \mathbf{p}_1^2 / \sigma) = \ln(1 + \mathbf{p}_2^2 / \sigma) = \dots = \ln(1 + \mathbf{p}_K^2 / \sigma) \Leftrightarrow \mathbf{p}_k \equiv \mathbf{p}_0$

A. Step descent algorithm

Let $\theta^{(\kappa)}$ be a point found during the $(\kappa - 1)$ -st iteration. The linearized function of f at $e^{j\theta^{(\kappa)}}$ is

$$3f(e^{j\theta^{(\kappa)}}) - 2\Re\{\langle \mathcal{H}^H(e^{j\theta^{(\kappa)}}) ([\mathcal{H}(e^{j\theta^{(\kappa)}})]^2)^{-2} \mathcal{H}(e^{j\theta^{(\kappa)}}) \rangle\} = 3f(e^{j\theta^{(\kappa)}}) - 2 \sum_{n=1}^N \Re\{e^{j\theta_n} \langle \mathcal{H}^H(e^{j\theta^{(\kappa)}}) \mathcal{A}^{(\kappa)} \mathcal{H}_n \rangle\}, \quad (13)$$

for

$$\mathcal{A}^{(\kappa)} \triangleq \left([\mathcal{H}(e^{j\theta^{(\kappa)}})]^2 \right)^{-2}. \quad (14)$$

We seek a step descent by addressing the following problem

$$\max_{\theta} \sum_{n=1}^N \Re\{e^{j\theta_n} \langle \mathcal{H}^H(e^{j\theta^{(\kappa)}}) \mathcal{A}^{(\kappa)} \mathcal{H}_n \rangle\}, \quad (15)$$

which is decomposed into N independent problems:

$$\max_{\theta_n} \Re\{e^{j\theta_n} \langle \mathcal{H}^H(e^{j\theta^{(\kappa)}}) \mathcal{A}^{(\kappa)} \mathcal{H}_n \rangle\}, n = 1, \dots, N,$$

each of which admits the closed-form solution

$$\tilde{\theta}_n^{(\kappa+1)} = -\angle \langle \mathcal{H}^H(e^{j\theta^{(\kappa)}}) \mathcal{A}^{(\kappa)} \mathcal{H}_n \rangle, n = 1, \dots, N. \quad (16)$$

We may then choose $\theta^{(\kappa+1)}$ according to one of the following rules:

- The simplest one

$$\theta^{(\kappa+1)} = \tilde{\theta}^{(\kappa+1)}. \quad (17)$$

- Considering $\psi^{(\kappa)} \triangleq \tilde{\theta}^{(\kappa+1)} - \theta^{(\kappa)}$ as a step descent, we update $\theta^{(\kappa+1)}$ according to the so-called Barzilai-Borwein (BB) step size of [25] in (18) and (19).
- Considering $\psi^{(\kappa)} \triangleq e^{j\tilde{\theta}^{(\kappa+1)}} - e^{j\theta^{(\kappa)}}$ we update $\theta^{(\kappa+1)}$ according to (20) and (21). We will refer this as the projective Barzilai-Borwein (PBB) step size.

Algorithm 1 provides the pseudo-code for the procedure iterating (17) or (19), or (21) in order to arrive at the computational solution of (12). The reader is referred to [25] for the rationale behind them in locating better feasible points, which are suitable for unconstrained optimization only. There is an explicit update of the incumbent point in Algorithm 1 because the updating rules (17)-(21) do not enhance that $\theta^{(\kappa)}$ is the incumbent. Somewhat surprisingly, the performance of Algorithm 1 was found to be indifferent with using any of three aforementioned rules.

Algorithm 1 ZFB step descent algorithm for (12)

- 1: **Initialization:** Initial $\theta^{(0)}$ and set $\theta^{opt} = \theta^{(0)}$ and $\gamma^{opt} = f(\theta^{opt})$ as the incumbent RIS and value.
 - 2: **Repeat until convergence of $\theta^{(\kappa)}$:** Generate $\tilde{\theta}^{(\kappa+1)}$ by (16). Then generate $\theta^{(\kappa+1)}$ either by (17) or (19), or (21). If $f(\theta^{(\kappa+1)}) < \gamma^{opt}$, set $\theta^{opt} = \theta^{(\kappa+1)}$ and $\gamma^{opt} = f(\theta^{(\kappa+1)})$. Set $\kappa := \kappa + 1$.
 - 3: **Output** θ^{opt} and γ^{opt} .
-

B. Full step descent algorithms

We express f in (12) as:

$$f(e^{j\theta}) = \alpha \|e^{j\theta}\|^2 - \left(\alpha \|e^{j\theta}\|^2 - \langle ([\mathcal{H}(e^{j\theta})]^2)^{-1} \rangle \right) \quad (22)$$

$$= \alpha N - g(e^{j\theta}), \quad (23)$$

where $\alpha > 0$ is chosen for ensuring that the function

$$g(e^{j\theta}) \triangleq \alpha \|e^{j\theta}\|^2 - \langle ([\mathcal{H}(e^{j\theta})]^2)^{-1} \rangle$$

is convex in $e^{j\theta}$. The problem (12) is equivalent to the following problem of unconstrained concave optimization [22]³

$$\max_{\theta} g(e^{j\theta}). \quad (24)$$

Following [26]–[28] we will develop a local Frank-and-Wolf (FW) feasible direction algorithm for solving this problem as it bypasses the line search to give as a full step size of length 1. Moreover, this kind of FW algorithm has proved to be very efficient in practice [29]. To this end, let $\theta^{(\kappa)}$ be a point found during the $(\kappa - 1)$ -st iteration. Note that as g is convex, its linearized function provides its lower bound formulated as:

$$g(e^{j\theta}) \geq \alpha \left(2\Re\left\{ \sum_{n=1}^N e^{j\theta_n} e^{-j\theta_n^{(\kappa)}} \right\} - N \right) - 3\langle ([\mathcal{H}(e^{j\theta^{(\kappa)}})]^2)^{-1} \rangle + 2\Re\left\{ \sum_{n=1}^N e^{j\theta_n} \langle \mathcal{H}^H(e^{j\theta^{(\kappa)}}) \mathcal{A}^{(\kappa)} \mathcal{H}_n \rangle \right\} \quad (25)$$

$$= -\alpha N - 3\langle ([\mathcal{H}(e^{j\theta^{(\kappa)}})]^2)^{-1} \rangle + 2 \sum_{n=1}^N \Re\{e^{j\theta_n} (\alpha e^{-j\theta_n^{(\kappa)}} + \langle \mathcal{H}^H(e^{j\theta^{(\kappa)}}) \mathcal{A}^{(\kappa)} \mathcal{H}_n \rangle)\} \quad (26)$$

$$\triangleq g^{(\kappa)}(e^{j\theta}),$$

where $\mathcal{A}^{(\kappa)}$ is defined in (14). For finding the FW feasible direction, we solve the following problem at the κ -th iteration to generate $\theta^{(\kappa+1)}$

$$\max_{\theta} 2 \sum_{n=1}^N \Re\{e^{j\theta_n} (\alpha e^{-j\theta_n^{(\kappa)}} + \langle \mathcal{H}^H(e^{j\theta^{(\kappa)}}) \mathcal{A}^{(\kappa)} \mathcal{H}_n \rangle)\}, \quad (27)$$

which admits the following closed-form solution similar to (16):

$$\theta_n^{(\kappa+1)} = -\angle \left(\alpha e^{-j\theta_n^{(\kappa)}} + \langle \mathcal{H}^H(e^{j\theta^{(\kappa)}}) \mathcal{A}^{(\kappa)} \mathcal{H}_n \rangle \right), \quad n = 1, \dots, N. \quad (28)$$

We can readily show that

$$g(e^{j\theta^{(\kappa+1)}}) \geq g^{(\kappa)}(e^{j\theta^{(\kappa+1)}}) > g^{(\kappa)}(e^{j\theta^{(\kappa)}}) = g(e^{j\theta^{(\kappa)}}), \quad (29)$$

so $\theta^{(\kappa+1)}$ is a better point than $\theta^{(\kappa)}$, i.e. $1 = \arg \max_{0 \leq \nu \leq 1} g(e^{j(\theta^{(\kappa)} + \nu(\theta^{(\kappa+1)} - \theta^{(\kappa)}))})$, so the full step size of length one is achieved.⁴ The associated pseudo-code is

³(24) is equivalent to $\min_{\theta} (-g(e^{j\theta}))$, where $-g(e^{j\theta})$ is a concave function

⁴Obviously, the step size is not full whenever $\arg \max_{0 \leq \nu \leq 1} g(e^{j(\theta^{(\kappa)} + \nu(\theta^{(\kappa+1)} - \theta^{(\kappa)}))}) < 1$

$$\theta^{(\kappa+1)} = \theta^{(\kappa)} + \frac{|\langle \psi^{(\kappa)}, \psi^{(\kappa)} - \psi^{(\kappa-1)} \rangle|}{\|\psi^{(\kappa)} - \psi^{(\kappa-1)}\|^2} \psi^{(\kappa)} \quad (18)$$

$$= \theta^{(\kappa)} + \frac{|\langle \tilde{\theta}^{(\kappa+1)} - \theta^{(\kappa)}, \tilde{\theta}^{(\kappa+1)} - \theta^{(\kappa)} - \tilde{\theta}^{(\kappa)} + \theta^{(\kappa-1)} \rangle|}{\|\tilde{\theta}^{(\kappa+1)} - \theta^{(\kappa)} - \tilde{\theta}^{(\kappa)} + \theta^{(\kappa-1)}\|^2} (\tilde{\theta}^{(\kappa+1)} - \theta^{(\kappa)}). \quad (19)$$

$$\theta^{(\kappa+1)} = \angle \left(e^{j\theta^{(\kappa)}} + \frac{|\langle \psi^{(\kappa)}, \psi^{(\kappa)} - \psi^{(\kappa-1)} \rangle|}{\|\psi^{(\kappa)} - \psi^{(\kappa-1)}\|^2} \psi^{(\kappa)} \right) \quad (20)$$

$$= \angle \left(e^{j\theta^{(\kappa)}} + \frac{|\langle e^{j\tilde{\theta}^{(\kappa+1)}} - e^{j\theta^{(\kappa)}}, e^{j\tilde{\theta}^{(\kappa+1)}} - e^{j\tilde{\theta}^{(\kappa)}} - e^{j\tilde{\theta}^{(\kappa)}} + e^{j\theta^{(\kappa-1)}} \rangle|}{\|e^{j\tilde{\theta}^{(\kappa+1)}} - e^{j\tilde{\theta}^{(\kappa)}} - e^{j\tilde{\theta}^{(\kappa)}} + e^{j\theta^{(\kappa-1)}}\|^2} (e^{j\tilde{\theta}^{(\kappa+1)}} - e^{j\theta^{(\kappa)}}) \right). \quad (21)$$

provided by Algorithm 2, which iterates incumbent points bypassing any line search. In contrast to Algorithm 1, the convergence of Algorithm 2 to at least a locally optimal solution of (24) can be readily proved [29].

Remark. To efficiently find a reasonable α in (22), we rely on the following procedure. Initialize the procedure by using a sufficiently large $\alpha^{(0)}$, solve (27) and update $\alpha^{(\kappa+1)} = \alpha^{(\kappa)}/10$ until not arrive at $g(e^{j\theta^{(\kappa+1)}}) \leq g(e^{j\theta^{(\kappa)}})$.

We also propose an alternative full step descent procedure for (12) by addressing the following problem of perturbed optimization:

$$\min_{\theta} f_{\alpha}(e^{j\theta}) \triangleq \langle ([\mathcal{H}(e^{j\theta})]^2 + \alpha I_K)^{-1} \rangle \quad (30)$$

for a sufficient small $\alpha > 0$. Using the matrix inverse formula (31) of (see e.g. [30]):

$$\begin{aligned} & \left([\mathcal{H}(e^{j\theta})]^2 + \alpha I_K \right)^{-1} \\ &= -\alpha^{-2} \mathcal{H}(e^{j\theta}) \left(I_M + \alpha^{-1} [\mathcal{H}^H(e^{j\theta})]^2 \right)^{-1} \mathcal{H}^H(e^{j\theta}) \\ & \quad + \alpha^{-1} I_K \\ &= -\alpha^{-1} \mathcal{H}(e^{j\theta}) \left(\alpha I_M + \mathcal{H}^H(e^{j\theta}) \mathcal{H}(e^{j\theta}) \right)^{-1} \mathcal{H}^H(e^{j\theta}) \\ & \quad + \alpha^{-1} I_K, \end{aligned} \quad (31)$$

the problem in (30) may be shown to be equivalent to

$$\max_{\theta} g_{\alpha}(e^{j\theta}) \triangleq \langle \mathcal{H}(e^{j\theta}) \left(\alpha I_M + [\mathcal{H}^H(e^{j\theta})]^2 \right)^{-1} \mathcal{H}^H(e^{j\theta}) \rangle. \quad (32)$$

Again, let $\theta^{(\kappa)}$ be a point found during the $(\kappa - 1)$ -st iteration. Exploiting the inequality (86) in the Appendix yields (33) for $\Psi^{(\kappa)} = \left(\alpha I_M + [\mathcal{H}^H(e^{j\theta^{(\kappa)}})]^2 \right)^{-1}$, $a^{(\kappa)} \triangleq -\alpha \langle [\mathcal{H}^H(e^{j\theta^{(\kappa)}})]^2 [\Psi^{(\kappa)}]^2 \rangle$, $b^{(\kappa)}(n) \triangleq \langle \mathcal{H}_n \Psi^{(\kappa)} \mathcal{H}^H(e^{j\theta^{(\kappa)}}) \rangle$, $n \in \mathcal{N}$, and $\mathcal{C}^{(\kappa)}(n, m) \triangleq \langle \mathcal{H}_n^H \mathcal{H}_m [\Psi^{(\kappa)} \mathcal{H}^H(e^{j\theta^{(\kappa)}})]^2 \rangle$, $(n, m) \in \mathcal{N} \times \mathcal{N}$, while $\lambda_{\max}(\mathcal{C}^{(\kappa)})$ is the maximum eigenvalue of $\mathcal{C}^{(\kappa)}$, which is positive because the matrix $\mathcal{C}^{(\kappa)}$ is positive definite.

We thus solve the following problem to generate $\theta^{(\kappa+1)}$

$$\max_{\theta} g_{\alpha}^{(\kappa)}(e^{j\theta}), \quad (34)$$

which admits the following closed-form solution similar to (16):

$$\theta_n^{(\kappa+1)} = -\angle(b^{(\kappa)}(n) - \sum_{m=1}^N e^{-j\theta_m^{(\kappa)}} \mathcal{C}^{(\kappa)}(m, n))$$

$$+ \lambda_{\max}(\mathcal{C}^{(\kappa)}) e^{-j\theta_n^{(\kappa)}}, n \in \mathcal{N}. \quad (35)$$

Similarly to (29), we can readily show that $g_{\alpha}(e^{j\theta^{(\kappa+1)}}) > g_{\alpha}(e^{j\theta^{(\kappa)}})$ as far as $\theta^{(\kappa+1)} \neq \theta^{(\kappa)}$, so (35) provides full step size update. A compact presentation of (34) is also included in Algorithm 2.

Before concluding this section, observe that after designing θ^{opt} , the throughput of all IUs is defined with the aid of (7) and (9) as

$$\ln \left(1 + \frac{P}{\sigma \langle ([\mathcal{H}(e^{j\theta^{opt}})]^2)^{-1} \rangle} \right). \quad (36)$$

Algorithm 2 ZFB full step descent algorithm

- 1: **Initialization:** Initial $\theta^{(0)}$.
- 2: **Repeat until convergence of $\theta^{(\kappa)}$:** Generate $\theta^{(\kappa+1)}$ by (28) or (35). Set $\kappa := \kappa + 1$.
- 3: **Output** $\theta^{opt} = \theta^{(\kappa)}$.

III. RIS-AIDED REGULARIZED ZERO-FORCING BEAMFORMING OPTIMIZATION

Now, whenever we have $K > M$, the matrix $\mathcal{H}(e^{j\theta}) \mathcal{H}^H(e^{j\theta})$ becomes singular and it cannot be inverted. Hence we cannot use the ZFB of (4). Instead, we consider RZFB, under which the BS transmits

$$\begin{aligned} x_I &= \mathcal{H}^H(e^{j\theta}) \left([\mathcal{H}(e^{j\theta})]^2 + \alpha I_K \right)^{-1} \text{diag}[\mathbf{p}_k]_{k=1, \dots, K} s \\ &= \left([\mathcal{H}^H(e^{j\theta})]^2 + \alpha I_M \right)^{-1} \mathcal{H}^H(e^{j\theta}) \text{diag}[\mathbf{p}_k]_{k=1, \dots, K} s \end{aligned} \quad (37)$$

The Equation (3) may be rewritten as

$$\begin{aligned} y &= \mathcal{H}(e^{j\theta}) \left([\mathcal{H}^H(e^{j\theta})]^2 + \alpha I_M \right)^{-1} \\ & \quad \mathcal{H}^H(e^{j\theta}) \text{diag}[\mathbf{p}_k]_{k=1}^K s + \tilde{n}. \end{aligned} \quad (38)$$

Thanks to the regularization of the ill-posed part only, we can design θ separately, because the capability of RZFB actually depends on the matrix

$$\begin{aligned}
g_\alpha(e^{j\theta}) &\geq -\alpha\langle[\mathcal{H}^H(e^{j\theta^{(\kappa)}})]^2[\Psi^{(\kappa)}]^2\rangle + 2\Re\{\langle\mathcal{H}(e^{j\theta})\Psi^{(\kappa)}\mathcal{H}^H(e^{j\theta^{(\kappa)}})\rangle\} - \langle[\mathcal{H}^H(e^{j\theta})]^2[\Psi^{(\kappa)}\mathcal{H}^H(e^{j\theta^{(\kappa)}})]^2\rangle \\
&= a^{(\kappa)} + 2\Re\left\{\sum_{n=1}^N e^{j\theta_n} b^{(\kappa)}(n)\right\} + (e^{j\theta})^H \mathcal{C}^{(\kappa)} e^{j\theta} \\
&\geq a^{(\kappa)} + 2\Re\left\{\sum_{n=1}^N e^{j\theta_n} \left(b^{(\kappa)}(n) - \sum_{m=1}^N e^{-j\theta_m^{(\kappa)}} \mathcal{C}^{(\kappa)}(m, n) + \lambda_{\max}(\mathcal{C}^{(\kappa)}) e^{-j\theta_n^{(\kappa)}}\right)\right\} - (e^{j\theta^{(\kappa)}})^H \mathcal{C}^{(\kappa)} e^{j\theta^{(\kappa)}} \\
&\quad - 2\lambda_{\max}(\mathcal{C}^{(\kappa)})N \\
&\triangleq g_\alpha^{(\kappa)}(e^{j\theta}), \tag{33}
\end{aligned}$$

$\mathcal{H}(e^{j\theta}) \left([\mathcal{H}^H(e^{j\theta})]^2 + \alpha I_M\right)^{-1} \mathcal{H}^H(e^{j\theta})$ in (38). Note that we have:

$$\begin{aligned}
&\preceq \begin{bmatrix} I_K & \mathcal{H}(e^{j\theta}) \\ \mathcal{H}^H(e^{j\theta}) & [\mathcal{H}^H(e^{j\theta})]^2 + \alpha I_M \end{bmatrix} \\
&= \begin{bmatrix} I_K & \mathcal{H}(e^{j\theta}) \\ \mathcal{H}^H(e^{j\theta}) & [\mathcal{H}^H(e^{j\theta})]^2 \end{bmatrix} \\
&= \begin{bmatrix} I_K \\ \mathcal{H}^H(e^{j\theta}) \end{bmatrix} [I_K \quad \mathcal{H}(e^{j\theta})] \succeq 0.
\end{aligned}$$

Upon using the Shur complement (see e.g. [30]), we arrive at:

$$I_K \succeq \mathcal{H}(e^{j\theta}) \left([\mathcal{H}^H(e^{j\theta})]^2 + \alpha I_M\right)^{-1} \mathcal{H}^H(e^{j\theta}). \tag{39}$$

It is plausible that the more similar the matrix in the right hand side (RHS) to the identity matrix in the left hand side (LHS), the better RZFB performs. Define an ellipsoid in \mathbb{C}^K :

$$\begin{aligned}
\mathcal{E}(\theta) &\triangleq \{x \in \mathbb{C}^K : x^H \mathcal{H}(e^{j\theta}) \left([\mathcal{H}^H(e^{j\theta})]^2 + \alpha I_M\right)^{-1} \\
&\quad \mathcal{H}^H(e^{j\theta}) x \leq 1\}. \tag{40}
\end{aligned}$$

The matrix inequality (39) shows that $\mathcal{E}(\theta)$ always contains the unit sphere:

$$\mathcal{E}(\theta) \supset \mathcal{U} \triangleq \{x \in \mathbb{C}^K : \|x\|^2 \leq 1\}. \tag{41}$$

The rest of this section is devoted to the optimization of θ based on optimizing the shape of $\mathcal{E}(\theta)$.

A. Trace-maximization based algorithm

We aim to minimize the surface of $\mathcal{E}(\theta)$, i.e. we aim to maximize the trace of the right hand side (RHS) of (39) [31]. As such, the problem is the same as (32), thus it may be solved by Alg. 2. We repeat it here as Algorithm 3 to emphasize that it is specifically tailored for RZFB.

Algorithm 3 RZF full step descent algorithm for trace maximization (32)

- 1: **Initialization:** Initial $\theta^{(0)}$.
 - 2: **Repeat until convergence of $\theta^{(\kappa)}$:** Generate $\theta^{(\kappa+1)}$ by (35). Set $\kappa := \kappa + 1$.
 - 3: **Output** θ^{opt} .
-

B. Determinant-maximization algorithms

We aim to minimize the volume of the set $\mathcal{E}(\theta) \setminus \mathcal{U}$, which is equivalent to the problem [31]:

$$\begin{aligned}
&\min_{\theta} |I_K - \mathcal{H}(e^{j\theta}) \left([\mathcal{H}^H(e^{j\theta})]^2 + \alpha I_M\right)^{-1} \mathcal{H}^H(e^{j\theta})| \\
&\Leftrightarrow \max_{\theta} \phi(e^{j\theta}) \triangleq \ln |I_K + \frac{1}{\alpha} [\mathcal{H}(e^{j\theta})]^2|, \tag{42}
\end{aligned}$$

because according to the matrix inversion formula, we have

$$\begin{aligned}
&I_K - \mathcal{H}(e^{j\theta}) \left([\mathcal{H}^H(e^{j\theta})]^2 + \alpha I_M\right)^{-1} \mathcal{H}^H(e^{j\theta}) \\
&= \left(I_K + \frac{1}{\alpha} [\mathcal{H}(e^{j\theta})]^2\right)^{-1}. \tag{43}
\end{aligned}$$

The problem (42) is equivalent to

$$\max_{\theta} \varphi(e^{j\theta}) \triangleq \ln |\alpha I_K + [\mathcal{H}(e^{j\theta})]^2|. \tag{44}$$

As always, let $\theta^{(\kappa)}$ be a point found during the $(\kappa - 1)$ -st iteration.

1) *Step descent algorithm:* The linearization of the function φ at $\theta^{(\kappa)}$ is formulated as:

$$\varphi(e^{j\theta^{(\kappa)}}) - \langle \mathcal{A}^{(\kappa)} [\mathcal{H}(e^{j\theta^{(\kappa)}})]^2 \rangle + \langle \mathcal{A}^{(\kappa)} [\mathcal{H}(e^{j\theta})]^2 \rangle, \tag{45}$$

for

$$\mathcal{A}^{(\kappa)} \triangleq \left(\alpha I_K + [\mathcal{H}(e^{j\theta^{(\kappa)}})]^2\right)^{-1}. \tag{46}$$

Thus, for $\mathcal{A}^{(\kappa)}$ defined by (46) we address the problem (13) and then (15) to generate the descent direction $\theta^{(\kappa+1)}$ given by (16) as per Algorithm 4, which has to update the incumbent point with the convergence not granted.

Algorithm 4 RZFB step descent algorithm for maximizing the log determinant (44)

- 1: **Initialization:** Initial $\theta^{(0)}$ and set $\theta^{opt} = \theta^{(0)}$ and $\eta^{opt} = \varphi(\theta^{opt})$ as the incumbent RIS and value.
 - 2: **Repeat until convergence of $\theta^{(\kappa)}$:** For $\mathcal{A}^{(\kappa)}$ defined by (46), generate $\theta^{(\kappa+1)}$ by (16). If $\varphi(\theta^{(\kappa+1)}) < \eta^{opt}$, set $\theta^{opt} = \theta^{(\kappa+1)}$ and $\eta^{opt} = \varphi(\theta^{(\kappa+1)})$. Set $\kappa := \kappa + 1$.
 - 3: **Output** θ^{opt} and η^{opt} .
-

$$\begin{aligned}
\phi(e^{j\theta}) &\geq \phi(e^{j\theta^{(\kappa)}}) - \|\mathcal{H}(e^{j\theta^{(\kappa)}})\|^2 + \frac{1}{\alpha} \left[2\Re\{\mathcal{H}(e^{j\theta})\mathcal{H}^H(e^{j\theta^{(\kappa)}})\} \right. \\
&\quad \left. - \langle \mathcal{H}(e^{j\theta^{(\kappa)}})(\alpha I_m + [\mathcal{H}^H(e^{j\theta^{(\kappa)}})]^2)^{-1}\mathcal{H}^H(e^{j\theta^{(\kappa)}}), [\mathcal{H}(e^{j\theta})]^2 \rangle \right] \\
&= a^{(\kappa)} + \frac{1}{\alpha} \left[2\Re\{\mathcal{H}(e^{j\theta})\mathcal{H}^H(e^{j\theta^{(\kappa)}})\} - \langle [\Psi^{(\kappa)}\mathcal{H}(e^{j\theta})]^2 \rangle \right] \\
&= a^{(\kappa)} + \frac{1}{\alpha} \left[2\Re\left\{ \sum_{n=1}^N e^{j\theta_n} b^{(\kappa)}(n) \right\} - (e^{j\theta})^H \mathcal{C}^{(\kappa)} e^{j\theta} \right] \\
&\geq a^{(\kappa)} + \frac{1}{\alpha} \left[2\Re\left\{ \sum_{n=1}^N e^{j\theta_n} \left(b^{(\kappa)}(n) - \sum_{m=1}^N e^{-j\theta_m^{(\kappa)}} \mathcal{C}^{(\kappa)}(m, n) + \lambda_{\max}(\mathcal{C}^{(\kappa)}) e^{-j\theta_n^{(\kappa)}} \right) \right\} \right. \\
&\quad \left. - (e^{j\theta^{(\kappa)}})^H \mathcal{C}^{(\kappa)} e^{j\theta^{(\kappa)}} - 2\lambda_{\max}(\mathcal{C}^{(\kappa)})N \right] \\
&\triangleq \phi^{(\kappa)}(e^{j\theta}), \tag{47}
\end{aligned}$$

2) *Full step descent algorithm:* We also can use the inequality (88) to address (42) as (47), for $a^{(\kappa)} \triangleq \phi(e^{j\theta^{(\kappa)}}) - \|\mathcal{H}(e^{j\theta^{(\kappa)}})\|^2$, $\Psi^{(\kappa)} \triangleq (\alpha I_m + [\mathcal{H}^H(e^{j\theta^{(\kappa)}})]^2)^{-1/2} \mathcal{H}^H(e^{j\theta^{(\kappa)}})$, $b^{(\kappa)}(n) \triangleq \langle \mathcal{H}_n \mathcal{H}^H(e^{j\theta^{(\kappa)}}) \rangle$, $n \in \mathcal{N}$, $\mathcal{C}^{(\kappa)}(n, m) \triangleq \langle \mathcal{H}_m \mathcal{H}_n^H [(\Psi^{(\kappa)})^H]^2 \rangle$, $(n, m) \in \mathcal{N} \times \mathcal{N}$, and $\lambda_{\max}(\mathcal{C}^{(\kappa)})$ is the maximum eigenvalue of $\mathcal{C}^{(\kappa)}$, which is positive because the matrix $\mathcal{C}^{(\kappa)}$ is positive definite.

We thus solve the following problem to generate a better point $\theta^{(\kappa+1)}$

$$\max_{\theta} \phi^{(\kappa)}(e^{j\theta}), \tag{48}$$

which admits the following closed-form solution similar to (16):

$$\begin{aligned}
\theta_n^{(\kappa+1)} &= -\angle(b^{(\kappa)}(n) - \sum_{m=1}^N e^{-j\theta_m^{(\kappa)}} \mathcal{C}^{(\kappa)}(m, n) \\
&\quad + \lambda_{\max}(\mathcal{C}^{(\kappa)}) e^{-j\theta_n^{(\kappa)}}), n \in \mathcal{N}. \tag{49}
\end{aligned}$$

Algorithm 5 RZF full step descent algorithm for maximizing the log determinant (44)

- 1: **Initialization:** Initial $\theta^{(0)}$.
- 2: **Repeat until convergence of $\theta^{(\kappa)}$:** Generate a better point $\theta^{(\kappa+1)}$ by (49). Set $\kappa := \kappa + 1$.
- 3: **Output** $\theta^{opt} = \theta^{(\kappa)}$.

Before concluding this section, let us mention that after designing θ^{opt} , we insert it into (38) to consider the problem of power allocation \mathbf{p}_k , $k = 1, \dots, K$ for max-min users rate optimization. However, we will treat it as a particular case of the problems in the next section.

IV. ZFB APPLICATIONS TO RIS-AIDED INTEGRATED DATA AND ENERGY DELIVERY

Now, in addition to IUs we consider a scenario with the BS serving also K_E EUs e_ℓ , $\ell \in \mathcal{K}_E \triangleq \{1, \dots, K_E\}$, which are located near the BS to harvest energy from the BS. We employ the transmit-TS technique, under which the first time-slot fraction $1/t_1$ is used for energy delivery and the second time-slot fraction $1/t_2$ is used for information delivery.

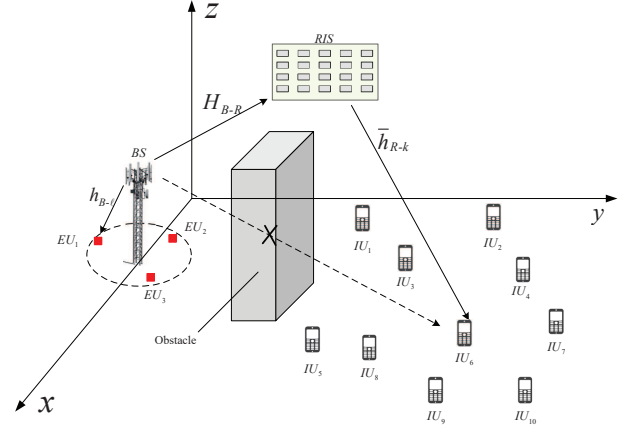


Fig. 3: Scenario setup for integrated data and energy networking.

A. Energy delivery during $1/t_1$

Let us assume that the LoS channel spanning from the BS to EU e_ℓ is $\tilde{h}_{B-e_\ell} \triangleq \sqrt{\beta_{B-e_\ell}^E} h_{B-e_\ell} \in \mathbb{C}^{1 \times M}$, where $\sqrt{\beta_{B-e_\ell}^E}$ models both the path-loss and the large-scale fading of the LoS component, where the entries of h_{B-e_ℓ} are $\mathcal{C}(0, 1)$, to modelling the small-scale fading.

The signal received at EU e_ℓ is

$$y_{e_\ell} = \tilde{h}_{B-e_\ell} x_E, \tag{50}$$

where $x_E \in \mathbb{C}^M$ is the transmitted signal carrying the energy. Note that in (50) we ignore the background noise, as its power is negligible for EH. Inspired by [6], conjugate energy beamforming is used, so we have

$$x_E = \sum_{\ell=1}^{K_E} \tilde{h}_{B-e_\ell}^H \sqrt{\mathbf{x}_\ell} \delta_\ell,$$

where $\delta_\ell \in \mathcal{C}(0, 1)$, which is the energy symbol. The power of the transmit energy signal is

$$\pi_E(\mathbf{x}) = \sum_{\ell=1}^{K_E} \|\tilde{h}_{B-e_\ell}\|^2 \mathbf{x}_\ell.$$

The energy harvested by EU e_ℓ during $1/t_1$ is $\zeta\pi_\ell(\mathbf{x})$ with

$$\pi_\ell(\mathbf{x}) \triangleq \frac{\sum_{\ell'=1}^{K_E} |\langle \tilde{\mathbf{h}}_{B-e_\ell}, \tilde{\mathbf{h}}_{B-e_{\ell'}} \rangle|^2 \mathbf{x}_{\ell'}}{t_1}, \quad (51)$$

while ζ is the efficiency of energy conversion, which is set to 0.5 in this paper.

B. Information transmission during $1/t_2$

The information transmission is implemented during the time-slot fraction $1/t_2$, with the signal received at IU k given by Equation (1), while the corresponding multi-input multi-output (MIMO) equation is given by (3). Since the specific design of PRCs has no impact on the EH performance, we insert θ^{opt} found in the previous sections into the equation (1) and (3) and also into (4) and (37) for ZFB or RZF beamforming, respectively. When the ZF beamformer of (4) is used in conjunction with $\mathbf{p}_k \equiv \mathbf{p}_0$, the throughput at IU k is expressed according to (7) as

$$r_0(\mathbf{p}_0) = \ln(1 + \mathbf{p}_0^2/\sigma), \quad (52)$$

and the power used for information transmission according to (9) is given by

$$a_{zf}\mathbf{p}_0^2 \quad (53)$$

for

$$a_{zf} \triangleq \langle ([\mathcal{H}(e^{j\theta^{opt}})]^2)^{-1} \rangle. \quad (54)$$

C. Optimal energy and ZF information beamforming

Here we consider the IUs' max-min throughput optimization problem subject to the QoES in terms of the EUs' harvested energy rate formulated as:

$$\max_{\mathbf{p}_0, \mathbf{x} \in \mathbb{R}_+^{K_E}, \gamma, \mathbf{t} = (t_1, t_2)^T \in \mathbb{R}_+^2} \gamma \quad \text{s.t.} \quad (55a)$$

$$\frac{\pi_E(\mathbf{x})}{t_1} + \frac{a_{zf}\mathbf{p}_0^2}{t_2} \leq P, \quad (55b)$$

$$\pi_E(\mathbf{x}) \leq 3P, a_{zf}\mathbf{p}_0^2 \leq 3P, \quad (55c)$$

$$\frac{1}{t_1} + \frac{1}{t_2} \leq 1, \quad (55d)$$

$$\sum_{\ell'=1}^{K_E} |\langle \tilde{\mathbf{h}}_{B-e_\ell}, \tilde{\mathbf{h}}_{B-e_{\ell'}}^H \rangle|^2 \mathbf{x}_{\ell'} \geq t_1 e_{\min}/\zeta, \ell \in \mathcal{K}_E, \quad (55e)$$

$$r_0(\mathbf{p}_0) \geq \gamma t_2, \quad (55f)$$

where e_{\min} is the harvested energy threshold. The slack variable γ is introduced in (55a) and (55f) to reflect the IUs' minimal throughput; (55b) is the total transmit power constraint under a given budget P and (55c) is a physical transmission constraint; (55d) restricts the energy and information transfer to a specific time slot, and (55e) represents the energy constraint of EUs in terms of their minimal required energy, which in fact reflects the following constraint:

$$\pi_\ell(\mathbf{x}) \geq e_{\min}/\zeta, \ell \in \mathcal{K}_E, \quad (56)$$

with $\pi_\ell(\mathbf{x})$ defined in (51).

In the problem (55), the constraints (55c)-(55e) are convex but the constraints (55b) and (55f) are not, making (55) a

nonconvex problem. We now develop inner convex approximations for these nonconvex constraints to propose a path-following algorithm for computing (55).

Let $(p_0^{(\kappa)}, x^{(\kappa)}, t^{(\kappa)}, \gamma^{(\kappa)})$ be a feasible point for (55) that is found from the $(\kappa - 1)$ -st iteration. Then upon using the following inequality

$$\pi_E(\mathbf{x}) \leq \pi_E^{(\kappa)}(\mathbf{x}) \triangleq \frac{1}{2} \left(\frac{\pi_E^2(\mathbf{x})}{\pi_E(x^{(\kappa)})} + \pi_E(x^{(\kappa)}) \right), \quad (57)$$

the nonconvex constraint (55b) is innerly approximated by

$$\frac{\pi_E^{(\kappa)}(\mathbf{x})}{t_1} + \frac{a_{zf}\mathbf{p}_0^2}{t_2} \leq P. \quad (58)$$

Using the inequality (87) yields the following concave quadratic minorant of $r_0(\mathbf{p}_0)$ in the LHS of (55f):⁵

$$r_0^{(\kappa)}(\mathbf{p}_0) \triangleq r_0^{(\kappa)}(p_0^{(\kappa)}) - \frac{(p_0^{(\kappa)})^2}{\sigma} + 2\frac{p_0^{(\kappa)}}{\sigma}\mathbf{p}_0 - \frac{(p_0^{(\kappa)})^2}{\sigma((p_0^{(\kappa)})^2 + \sigma)}(\mathbf{p}_0^2 + \sigma). \quad (59)$$

Meanwhile, the RHS of (55f) is upper bounded as follows:

$$\gamma t_2 \leq \frac{\gamma^{(\kappa)} t_2^{(\kappa)}}{4} \left(\frac{\gamma}{\gamma^{(\kappa)}} + \frac{t_2}{t_2^{(\kappa)}} \right)^2. \quad (60)$$

The nonconvex constraint (55f) is thus innerly approximated by the following convex quadratic constraint

$$r_0^{(\kappa)}(\mathbf{p}_0) \geq \frac{\gamma^{(\kappa)} t_2^{(\kappa)}}{4} \left(\frac{\gamma}{\gamma^{(\kappa)}} + \frac{t_2}{t_2^{(\kappa)}} \right)^2. \quad (61)$$

We then solve the following convex optimization problem for generating the next feasible point $(p_0^{(\kappa+1)}, x^{(\kappa+1)}, t^{(\kappa+1)}, \gamma^{(\kappa+1)})$ for (55):

$$\max_{\mathbf{p}_0, \mathbf{x}, \gamma, \mathbf{t} = (t_1, t_2)^T \in \mathbb{R}_+^2} \gamma \quad \text{s.t.} \quad (55c), (55d), (55e), (58), (61). \quad (62)$$

As this convex problem involves $m_c = K_E + 3$ decision variables and $n_v = 5$ quadratic constraints, its computational complexity is on the order of [32]

$$\mathcal{O}[m_c^{2.5}(n_v^2 + m_c)]. \quad (63)$$

As $(p_0^{(\kappa+1)}, x^{(\kappa+1)}, t^{(\kappa+1)}, \gamma^{(\kappa+1)})$ is the optimal solution of (62), while $(p_0^{(\kappa+1)}, x^{(\kappa)}, t^{(\kappa)}, \gamma^{(\kappa)})$ is its feasible point, it follows that

$$\gamma^{(\kappa+1)} > \gamma^{(\kappa)}, \quad (64)$$

provided that $(p_0^{(\kappa+1)}, x^{(\kappa+1)}, t^{(\kappa+1)}, \gamma^{(\kappa+1)}) \neq (p_0^{(\kappa)}, x^{(\kappa)}, t^{(\kappa)}, \gamma^{(\kappa)})$, i.e. $(p_0^{(\kappa+1)}, x^{(\kappa+1)}, t^{(\kappa+1)}, \gamma^{(\kappa+1)})$ is a better feasible point than $(p_0^{(\kappa)}, x^{(\kappa)}, t^{(\kappa)}, \gamma^{(\kappa)})$. The sequence $\{(p_0^{(\kappa)}, x^{(\kappa)}, t^{(\kappa)}, \gamma^{(\kappa)})\}$ of improved feasible points for (55) converges at least to a locally optimal solution of (55). As analyzed in [3], this locally optimal solution often turns out to be the globally optimal one. Algorithm 6 provides the pseudo-code for the procedure iterating (62).

$${}^5 r_0(\mathbf{p}_0) \geq r_0^{(\kappa)}(\mathbf{p}_0)$$

Algorithm 6 ZF Path-following algorithm for (55)

- 1: **Initialization:** Randomly generate a feasible point $(p_0^{(0)}, x^{(0)}, t^{(0)}, \gamma^{(0)})$ for (55). Set $\kappa = 0$.
 - 2: **Repeat until convergence of $\gamma^{(\kappa)}$:** Generate $(p_0^{(\kappa+1)}, x^{(\kappa+1)}, t^{(\kappa+1)}, \gamma^{(\kappa+1)})$ by solving the convex problem (62). Set $\kappa := \kappa + 1$.
 - 3: **Output** $(p_0^{(\kappa)}, x^{(\kappa)}, t^{(\kappa)}, \gamma^{(\kappa)})$.
-

V. RZFB APPLICATIONS TO RIS-AIDED INTEGRATED DATA AND ENERGY DELIVERY

A. The conventional RZFB

When the RZFB (37) is used, Equation (38) becomes

$$y_k = \bar{h}_{B-k} \bar{\mathcal{H}}^{rz} \sum_{j=1}^K \bar{h}_{B-j}^H \mathbf{p}_j s_j + \bar{n}_k \quad (65)$$

$$= \sum_{j=1}^K \bar{h}_{kj} \mathbf{p}_j s_j + \bar{n}_k, \quad (66)$$

for

$$\begin{aligned} \bar{\mathcal{H}}^{rz} &\triangleq (\mathcal{H}^H(\theta^{opt}) \mathcal{H}(\theta^{opt}) + \alpha I_M)^{-1} \\ \bar{h}_{B-j} &\triangleq h_{B-j}(\theta^{opt}), j = 1, \dots, K. \end{aligned} \quad (67)$$

and

$$\bar{h}_{kj} \triangleq \bar{h}_{B-k} \bar{\mathcal{H}}^{rz} \bar{h}_{B-j}^H. \quad (68)$$

The throughput at IU k is expressed as:

$$r_k(\mathbf{p}) = \ln \left(1 + |\bar{h}_{kk}|^2 \mathbf{p}_k^2 \left(\sum_{j \neq k} |\bar{h}_{kj}|^2 \mathbf{p}_j^2 + \sigma \right)^{-1} \right). \quad (69)$$

The transmit power apportioned for information delivery is

$$\pi_I(\mathbf{p}) \triangleq \sum_{j=1}^K \|\bar{\mathcal{H}}^{rz} \bar{h}_{B-j}^H\|^2 \mathbf{p}_j^2. \quad (70)$$

Thus we consider the following problem of the IUs' max-min throughput optimization subject to the QoES in terms of the EUs' harvested energy thresholds:

$$\max_{\mathbf{p}, \mathbf{x}, \gamma, \mathbf{t}=(t_1, t_2) \in \mathbb{R}_+^2} \gamma \quad \text{s.t.} \quad (55d), (55e), \quad (71a)$$

$$\frac{\pi_E(\mathbf{x})}{t_1} + \frac{\pi_I(\mathbf{p})}{t_2} \leq P, \quad (71b)$$

$$\pi_E(\mathbf{x}) \leq 3P, \pi_I(\mathbf{p}) \leq 3P, \quad (71c)$$

$$r_k(\mathbf{p}) \geq \gamma t_2, k \in \mathcal{K}, \quad (71d)$$

where like their counterparts in (55), γ in (71a) and (71d) is a slack variable to express the IUs minimal throughput, (71b) and (71c) are respectively the total power transmit constraint under the budget P and a physical transmission constraint, while as before, (55d) restricts the energy and information transfer within a time slot, and (55e) is the energy constraint of EUs in terms of their minimal required energy.

To propose a path-following algorithm for computing (71), we have to develop inner approximations for its nonconvex constraints (71b) and (71d).

Let $(p^{(\kappa)}, x^{(\kappa)}, t^{(\kappa)}, \gamma^{(\kappa)})$ be a feasible point for (71) that is found from the $(\kappa - 1)$ -st iteration. Based on the inequality (57), the nonconvex constraint (71b) is innerly approximated by

$$\frac{\pi_E(\mathbf{x})}{t_1} + \frac{\pi_I(\mathbf{p})}{t_2} \leq P. \quad (72)$$

Using the inequality (87) yields the following concave quadratic minorant of $r_k(\mathbf{p})$ in the LHS of (71d):

$$r_k^{(k)}(\mathbf{p}) \triangleq \tilde{a}^{(k)} + 2\tilde{b}^{(k)} \mathbf{p}_k - \tilde{c}^{(k)} \sum_{j=1}^K |\bar{h}_{kj}|^2 \mathbf{p}_j^2, \quad (73)$$

where

$$\begin{aligned} \tilde{a}_k^{(k)} &= r_k(p^{(\kappa)}) - |\bar{h}_{kk}|^2 (p_k^{(\kappa)})^2 \left(\sum_{j \neq k} |\bar{h}_{kj}|^2 (p_j^{(\kappa)})^2 + \sigma \right)^{-1} \\ &\quad - \sigma \tilde{c}_k^{(k)}, \\ \tilde{b}_k^{(k)} &= |\bar{h}_{kk}|^2 p_k^{(\kappa)} \left(\sum_{j \neq k} |\bar{h}_{kj}|^2 (p_j^{(\kappa)})^2 + \sigma \right)^{-1}, \\ \tilde{c}_k^{(k)} &= \left(\sum_{j \neq k} |\bar{h}_{kj}|^2 (p_j^{(\kappa)})^2 + \sigma \right)^{-1} - \left(\sum_{j=1}^K |\bar{h}_{kj}|^2 (p_j^{(\kappa)})^2 + \sigma \right)^{-1}. \end{aligned}$$

By (60) and (73), the nonconvex constraint (71d) is innerly approximated by the following convex quadratic constraint

$$r_k^{(k)}(\mathbf{p}) \geq \frac{\gamma^{(\kappa)} t_2^{(\kappa)}}{4} \left(\frac{\gamma}{\gamma^{(\kappa)}} + \frac{t_2}{t_2^{(\kappa)}} \right)^2, k \in \mathcal{K}. \quad (74)$$

We then solve the following convex optimization problem for generating the next feasible point $(p^{(\kappa+1)}, x^{(\kappa+1)}, t^{(\kappa+1)}, \gamma^{(\kappa+1)})$ for (71):

$$\max_{\mathbf{p}, \mathbf{x}, \gamma, \mathbf{t}=(t_1, t_2) \in \mathbb{R}_+^2} \gamma \quad \text{s.t.} \quad (55d), (55e), (71c), (72), (74). \quad (75)$$

The computational complexity order of this convex problem is given by (63) where we have $n_v = K + K_E + 3$ and $m_c = K + 4$. As $(p^{(\kappa+1)}, x^{(\kappa+1)}, t^{(\kappa+1)}, \gamma^{(\kappa+1)})$ is the optimal solution of (75) while $(p^{(\kappa)}, x^{(\kappa)}, t^{(\kappa)}, \gamma^{(\kappa)})$ is its feasible point, (64) is satisfied, provided that $(p^{(\kappa+1)}, x^{(\kappa+1)}, t^{(\kappa+1)}, \gamma^{(\kappa+1)}) \neq (p^{(\kappa)}, x^{(\kappa)}, t^{(\kappa)}, \gamma^{(\kappa)})$, i.e. $(p^{(\kappa+1)}, x^{(\kappa+1)}, t^{(\kappa+1)}, \gamma^{(\kappa+1)})$ is a better feasible point than $(p^{(\kappa)}, x^{(\kappa)}, t^{(\kappa)}, \gamma^{(\kappa)})$. The sequence $\{(p^{(\kappa)}, x^{(\kappa)}, t^{(\kappa)}, \gamma^{(\kappa)})\}$ of improved feasible points for (71) converges at least to a locally optimal solution of (71). Algorithm 7 provides the pseudo-code for solving (71) by iterating the convex problem (75).

B. New RZFB

Instead of (37), let us now design the transmit signal as

$$x_I = \bar{\mathcal{H}}^{rz} \sum_{j=1}^K \bar{h}_{B-j}^H [\mathbf{p}_{1,j} s_j + \mathbf{p}_{2,j} s_j^*] \quad (76)$$

Algorithm 7 Conventional RZF Path-following algorithm for (71)

- 1: **Initialization:** Randomly generate a feasible point $(p^{(0)}, x^{(0)}, t^{(0)}, \gamma^{(0)})$ for (71). Set $\kappa = 0$.
 - 2: **Repeat until convergence of $\gamma^{(\kappa)}$:** Generate $(p^{(\kappa+1)}, x^{(\kappa+1)}, t^{(\kappa+1)}, \gamma^{(\kappa+1)})$ by solving the convex problem (75). Set $\kappa := \kappa + 1$.
 - 3: **Output** $(p^{(\kappa)}, x^{(\kappa)}, t^{(\kappa)}, \gamma^{(\kappa)})$.
-

with $\mathbf{p}_{1,j} \in \mathbb{C}$ and $\mathbf{p}_{2,j} \in \mathbb{C}$, so instead of (66) the received signal by IU k is

$$y_k = \sum_{j=1}^K \bar{h}_{kj} [\mathbf{p}_{1,j} s_j + \mathbf{p}_{2,j} s_j^*] + \bar{n}_k. \quad (77)$$

While x_I defined by (37) is a proper Gaussian random variable with $\mathbb{E}((x_I)^2) = 0$, that defined by (76) is an improper Gaussian random variable [33] with $\mathbb{E}((x_I)^2) \neq 0$. The augmented form of (77) is

$$\bar{y}_k = \sum_{k=1}^K \bar{H}_{kj} V(\mathbf{p}_j) \bar{s}_j + \bar{n}_k^A, \quad (78)$$

where

$$\bar{y}_k \triangleq \begin{bmatrix} y_k \\ y_k^* \end{bmatrix}, \bar{H}_{kj} = \begin{bmatrix} \bar{h}_{kj} & 0 \\ 0 & \bar{h}_{kj}^* \end{bmatrix}, \bar{s}_j \triangleq \begin{bmatrix} s_j \\ s_j^* \end{bmatrix}, \bar{n}_k^A \triangleq \begin{bmatrix} \bar{n}_k \\ \bar{n}_k^* \end{bmatrix},$$

and

$$V(\mathbf{p}_j) \triangleq \begin{bmatrix} \mathbf{p}_{1,j} & \mathbf{p}_{2,j} \\ \mathbf{p}_{2,j}^* & \mathbf{p}_{1,j}^* \end{bmatrix}, \mathbf{p}_j \triangleq (\mathbf{p}_{1,j}, \mathbf{p}_{2,j}).$$

The throughput of IU k is $\frac{1}{2} \rho_k(\mathbf{p})$ [34] with

$$\rho_k(\mathbf{p}) \triangleq \ln \left| I_2 + [\bar{H}_{kk} V(\mathbf{p}_k)]^2 \left(\sum_{j \neq k} [\bar{H}_{kj} V(\mathbf{p}_j)]^2 + \sigma I_2 \right)^{-1} \right|.$$

The transmit power apportioned for information delivery is

$$\tilde{\pi}_I(\mathbf{p}) \triangleq \sum_{j=1}^K \|\bar{\mathcal{H}}^{Tz} \bar{h}_{B-j}^H [\mathbf{p}_{1,j} \quad \mathbf{p}_{2,j}]\|^2. \quad (79)$$

Thus we consider the following problem of the IUs' max-min rate optimization subject to the QoS in terms of the EUs' harvested energy thresholds corresponding to (71):

$$\max_{\mathbf{p}, \mathbf{x}, \gamma, \mathbf{t}=(t_1, t_2)^T \in \mathbb{R}_+^2} \gamma \quad \text{s.t.} \quad (55d), (55e), \quad (80a)$$

$$\frac{\pi_E(\mathbf{x})}{t_1} + \frac{\tilde{\pi}_I(\mathbf{p})}{t_2} \leq P, \quad (80b)$$

$$\pi_E(\mathbf{x}) \leq 3P, \tilde{\pi}_I(\mathbf{p}) \leq 3P, \quad (80c)$$

$$\rho_k(\mathbf{p}) \geq 2\gamma t_2, k \in \mathcal{K}. \quad (80d)$$

where like their counterparts in (71), the slack variable γ is introduced in (80a) and (80d) to express the IUs' minimal throughput, (80b) and (80c) are respectively the total power transmit constraint under the budget P and a physical transmission constraint, while as before, (55d) restricts the energy and information transfer within a time slot, and (55e) is the energy constraint of EUs in terms of their minimal

required energy. To propose a path-following algorithm for computing (80), we have to develop inner approximations for its nonconvex constraints (80b) and (80d).

Let $(p^{(\kappa)}, x^{(\kappa)}, t^{(\kappa)}, \gamma^{(\kappa)})$ be a feasible point for (71) that is found from the $(\kappa - 1)$ -st iteration.

Using the inequality (87) in the Appendix yields

$$\begin{aligned} \rho_k(\mathbf{p}) &\geq a_k^{(\kappa)} + 2\Re\{\langle V^H(p_k^{(\kappa)}) \bar{H}_{kk}^H (B_k^{(\kappa)})^{-1} \bar{H}_{kk} V(\mathbf{p}_k) \rangle\} \\ &\quad - \sum_{j=1}^K \|(C^{(\kappa)})^{1/2} \bar{H}_{kj} V(\mathbf{p}_j)\|^2 \\ &\triangleq \rho_k^{(k)}(\mathbf{P}), \end{aligned} \quad (81)$$

where

$$\begin{aligned} a_k^{(\kappa)} &\triangleq r_k(p^{(\kappa)}) - \langle [\bar{H}_{kk} V(p_k^{(\kappa)})]^2 (B_k^{(\kappa)})^{-1} \rangle - \sigma \langle C_k^{(\kappa)} \rangle, \\ B_k^{(\kappa)} &\triangleq \sum_{j \neq k} [\bar{H}_{kj} V(p_j^{(\kappa)})]^2 + \sigma I_2, \\ C_k^{(\kappa)} &\triangleq (B_k^{(\kappa)})^{-1} - \left(B_k^{(\kappa)} + [\bar{H}_{kk} V(p_k^{(\kappa)})]^2 \right)^{-1}. \end{aligned}$$

We then solve the following convex problem for generating the next better feasible point $(p^{(\kappa+1)}, x^{(\kappa+1)})$ for (80):

$$\begin{aligned} &\max_{\mathbf{p}, \mathbf{x}, \gamma, \mathbf{t}=(t_1, t_2)^T \in \mathbb{R}_+^2} \gamma \\ \text{s.t.} & \quad (55d), (55e), (72), (80b), (80c), \end{aligned} \quad (82a)$$

$$\rho_k^{(k)}(\mathbf{p}) \geq \frac{\gamma^{(\kappa)} t_2^{(\kappa)}}{2} \left(\frac{\gamma}{\gamma^{(\kappa)}} + \frac{t_2}{t_2^{(\kappa)}} \right)^2. \quad (82b)$$

The computational complexity order of this convex problem is given by (63) for $n_v = 2K + K_E + 3$ and $m_c = K + 4$. The pseudo-code for iterating (82) for computing (80) is provided by Algorithm 8.

Algorithm 8 New RZF Path-following algorithm for (80)

- 1: **Initialization:** Randomly generate a feasible point $(p^{(0)}, x^{(0)}, t^{(0)}, \gamma^{(0)})$ for (80). Set $\kappa = 0$.
 - 2: **Repeat until convergence of $\gamma^{(\kappa)}$:** Generate $(p^{(\kappa+1)}, x^{(\kappa+1)}, t^{(\kappa+1)}, \gamma^{(\kappa+1)})$ by solving the convex problem (82). Set $\kappa := \kappa + 1$.
 - 3: **Output** $(p^{(\kappa)}, x^{(\kappa)}, t^{(\kappa)}, \gamma^{(\kappa)})$.
-

C. Notices on RZFB for information delivery only

When $K_E = 0$, i.e. there are no EUs, we use the whole time-slot for information transfer. Hence we have $t_2 = 1$, i.e. the problems (71) and (80) are respectively reduced to

$$\max_{\mathbf{P}} \min_{k=1, \dots, K} r_k(\mathbf{p}) \quad \text{s.t.} \quad \pi_I(\mathbf{p}) \leq P, \quad (83)$$

and

$$\max_{\mathbf{P}} \min_{k=1, \dots, K} \rho_k(\mathbf{p}) \quad \text{s.t.} \quad \tilde{\pi}_I(\mathbf{p}) \leq P. \quad (84)$$

Algorithms 7 and 8 are directly adjusted for their computation. The pseudo-code is provided by Algorithm 9.

Algorithm 9 Path-following algorithm for (83)/(84)

- 1: **Initialization:** Randomly generate a feasible point $p^{(0)}$ for (83)/(84). Set $\kappa = 0$.
 - 2: **Repeat until convergence of $\gamma^{(\kappa)}$:** Generate $p^{(\kappa+1)}$ by solving the convex problem $\max_{\mathbf{p}} \min_{k=1, \dots, K} r_k^{(\kappa)}(\mathbf{p})$ s.t. $\pi_I(\mathbf{p}) \leq P$ (for computing (83)) and $\max_{\mathbf{p}} \min_{k=1, \dots, K} \rho_k^{(\kappa)}(\mathbf{p})$ s.t. $\tilde{\pi}_I(\mathbf{p}) \leq P$ (for computing (84)) Set $\kappa := \kappa + 1$.
 - 3: **Output $p^{(\kappa)}$.**
-

VI. NUMERICAL EXAMPLES

In this section, we investigate the performance of our proposed algorithms by numerical examples. The elements of the BS-to-RIS LoS channel matrix are generated by $[H_{B-R}]_{n,m} = e^{j\pi((n-1)\sin\bar{\theta}_n \sin\bar{\phi}_n + (m-1)\sin e^{j\theta_n} \sin\phi_n)}$, where $e^{j\theta_n}$ and ϕ_n are uniformly distributed as $e^{j\theta_n} \sim \mathcal{U}(0, \pi)$ and $\phi_n \sim \mathcal{U}(0, 2\pi)$, respectively, and $\bar{\theta}_n = \pi - \theta_n$ and $\bar{\phi}_n = \pi + \phi_n$ [14]. The normalized small-scale fading channel $h_{B-e\ell}$ spanning from the BS to EU ℓ and \bar{h}_{R-k} of the RIS to IU k obeys Rician distribution with a K-factor of 3 for modeling the LoS channels. The large scale fading coefficients, β_{B-R} , β_{R-k} , and $\beta_{B-e\ell}^E$, are modeled as [6], [14]

$$\begin{aligned} \beta_{B-R} &= G_{\text{BS}} + G_{\text{RIS}} - 35.9 - 22 \log_{10}(d_{B-R}) \text{ (in dB)}, \\ \beta_{R-k} &= G_{\text{RIS}} - 33.05 - 30 \log_{10}(d_{\text{RIS}-k}) \text{ (in dB)}, \\ \beta_{B-e\ell}^E &= G_{\text{BS}} - 30 - 20 \log_{10}(d_{B-e\ell}) \text{ (in dB)}, \end{aligned}$$

where $G_{\text{BS}} = 5$ dBi and $G_{\text{RIS}} = 5$ dBi denote the antenna gain of the BS and the RIS gain, respectively, while d_{B-R} , $d_{\text{RIS}-k}$, and $d_{B-e\ell}$ are the distances between the BS and RIS, the RIS and IU k , and the BS and EU ℓ , respectively. The signal reflected by the RIS can be ignored for EUs, since $\beta_{B-R}\beta_{R-k} \ll \beta_{B-e\ell}^E$. The spatial correlation matrix is given by $[\mathbf{R}_{\text{RIS}-k}]_{n,n'} = e^{j\pi(n-n')\sin\bar{\phi}_k \sin\bar{\theta}_k}$, where $\bar{\phi}_k$ and $\bar{\theta}_k$ are the azimuth and elevation angle for IU k , respectively. Unless otherwise stated, $K = 10$, $K_E = 3$, $e_0 = -20$ dBm and $N = 100$ are used. The results are multiplied by $\log_2 e$ to convert units of nats/sec into units of bps/Hz. The convergence tolerance of the proposed algorithms is set to 10^{-3} . All simulations implemented on a Core i7-10875H 2.30GHz processor.

We use the 3D coordinates (x, y, z) to locate all the objects concerned. The BS is at $(20, 0, 10)$, the RIS is at $(0, 30, 40)$.

A. RIS-aided information delivery

There are $K = 10$ IUs, which are randomly placed in a $60m \times 60m$ area RHS of the obstacle and the RIS. Unless stated otherwise, the transmit power of $P = 25$ dBm is used. The performance of Algorithm 1 is not sensitive to which step size from Equation (17), (19) and (21) is used. In the simulated figures, Alg 2A and Alg 2B refer to the performance of the full step descent algorithm 2 based on iterating (28) and (35), respectively. Alg 3, Alg 4 and Alg 5 respectively refer to the performance of Algorithm 3 for the trace-maximization (32), Algorithm 4 and Algorithm 5 for the

log determinant maximization (44). ZFB random θ and RZFB random θ respectively refer to the performance of ZFB and RZFB under random PRCs.

Fig. 4 and Fig. 5 plot the achievable minimum throughput versus the number of BS antennas, M under ZFB and RZFB, respectively.

Regarding ZFB for $M > K$, Fig. 4 reveals that Algorithm 2A outperforms Algorithm 2B, and the latter outperforms Algorithm 1, showing that the concave optimization reformulation (23) is the best option for computing (12), while Algorithm 1 of common purpose step descent is inefficient. Furthermore, the average running time for Algorithm 1, Algorithm 2A and Algorithm 2B are 0.24s, 0.06s and 7.96s under $N = 100$, respectively.

Regarding RZFB for $M > K$, Fig. 5 shows that Algorithm 3 achieves the best performance, i.e. the trace-maximization (32) has a more beneficial impact on the IUs' throughput than the log determinant maximization (44). It is not surprising to see that Algorithm 5 outperforms Algorithm 4 because the former iterates the incumbent points, while the latter simply provides a way to locate a beneficial direction.

The worst performance is attained by ZFB random θ and RZFB random θ in all figures which is a clear indication that the PRC optimization is absolutely necessary upon using RIS.

B. RIS-aided information and energy delivery

Next, we consider the problem of RIS-aided information and energy delivery by the network of Fig. 3 with $K_E = 3$ EUs randomly placed within a radius of 10m from the BS.

Alg 1-PGS, Alg 2A-PGS, Alg 2B-PGS and ZFB random θ -PGS refer to the performance of Algorithm 1, Algorithm 2A, Algorithm 2B, and ZFB random θ . Alg 3-PGS, Alg 4-PGS, Alg 5-PGS, and RZFB random θ -PGS refer to the performance of Algorithm 3, Algorithm 4, Algorithm 5, and RZFB random θ under RZFB (37), while Alg 3-IGS, Alg 4-IGS and Alg 5-IGS refer to the performance of Algorithm 3, Algorithm 4, Algorithm 5 under the new RZFB (76).

The transmit power of $P = 31$ dBm is set in Fig. 7-Fig. 9 and Fig. 11, but $P = 35$ dBm is set in Fig. 10 due to the relative small numbers of BS antennas.

Fig. 6 and Fig. 7 plot the minimum achievable IU throughput versus the number M of BS antennas under ZFB and RZFB, respectively. In Fig. 6, Alg 2A-PGS outperforms Alg 1-PGS and Alg 2B-PGS, Alg 2B-PGS outperforms Alg 1-PGS. Furthermore, all the proposed algorithms outperform ZFB random θ -PGS. As expected, Figures 5 and 7 exhibit similar trend. Fig. 6 and Fig. 7 also confirm the gain achieved by optimizing the PRCs. Furthermore, all algorithms in Fig. 4, Fig. 5, Fig. 6 and Fig. 7 benefit from the spatial diversity, which is commensurate with the number BS antennas.

In Fig. 8, we now examine the minimum achievable IU throughput upon varying the BS transmit power budget P under RZFB for $M = 10$. As expected, the IUs' minimum throughput increases upon increasing the available power budget due to the availability of more power for information delivery. Naturally, beyond a certain threshold, namely $P = 40$ dBm in Fig. 8, Alg 3's performance becomes saturated because

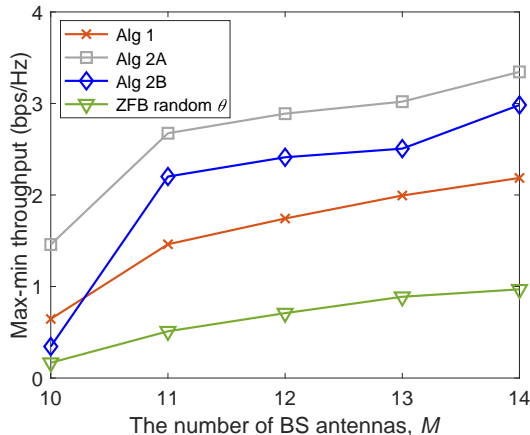


Fig. 4: Achievable minimum throughput vs the number of BS antennas M under ZF.

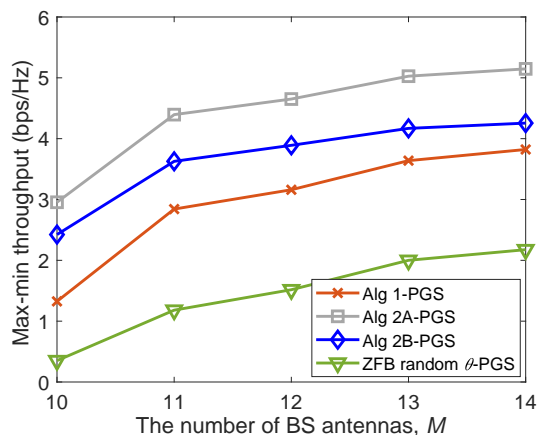


Fig. 6: Achievable minimum throughput vs the number of BS antennas M under ZF.

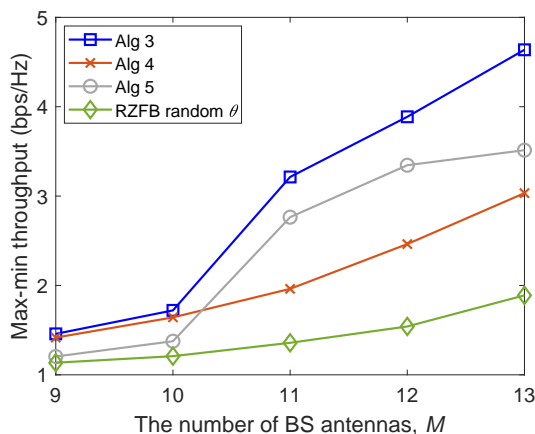


Fig. 5: Achievable minimum throughput vs the number of BS antenna M under RZF.

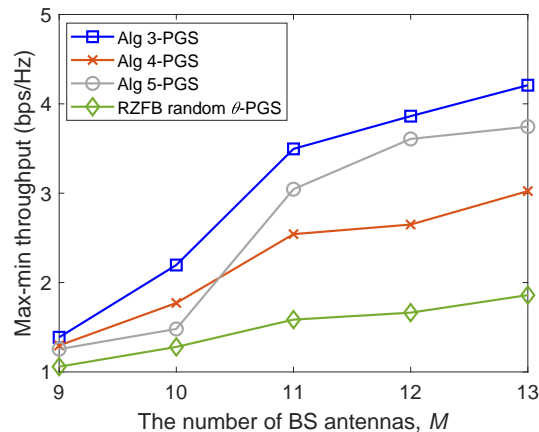


Fig. 7: Achievable minimum throughput vs the number of BS antennas M under RZF.

the network is interference-limited. Fig. 8 also shows the gap between Algorithm 5 and RZFB under random θ , which is quite narrow for $P \geq 34$ dBm because the beneficial impact of the RIS is reduced, when the power budget is increased.

Fig. 9 plots the achievable minimum IU throughput for $M = 10$ under RZF versus the number N of RIS reflecting elements, showing that the performance is improved upon increasing N .

Fig. 10 and Fig. 11 allow us to compare the performance achieved by the RZFB (76) and the new RZFB (82). Fig. 10 plots the achievable minimum IU throughput versus the number M of BS antennas, clearly showing that Alg 3-IGS outperforms its counterpart Alg 3-PGS. Similarly, Alg 4-IGS and Alg 5-IGS outperform their counterparts Alg 4-PGS and Alg 5-PGS. Fig. 11, which plots the achievable minimum IU throughput for $K = M + 1$, follow the same trend as Fig. 10: Alg 3-IGS, Alg 4-IGS and Alg 5-IGS outperform their counterparts Alg 3-PGS, Alg 4-PGS and Alg 5-PGS, respectively. The advantage of the new RZFB over the conventional RZFB is also confirmed. Furthermore, Algorithm 4 benefits to a lesser extent from the new RZFB than Algorithm 3 and Algorithm 5.

TABLE I: The average number of iterations required for the algorithm's convergence

	$M = 5$	$M = 6$	$M = 7$	$M = 8$	$M = 9$
Alg 3-PGS	15	14	14	10	9
Alg 4-PGS	10	9	8	8	8
Alg 5-PGS	17	16	17	14	11
Alg 3-IGS	17	16	17	14	13
Alg 4-IGS	17	15	15	15	11
Alg 5-IGS	23	21	23	17	12

Finally, Table I provides the average number of required iterations for the convex optimization part of the algorithms' convergence in simulating Fig. 9. The average single iteration time is 3.02s and 4.83s for the PGS based and IGS based algorithms, respectively. All the algorithms only need 30% of the maximum number of iterations to reach 80% of their optimal values.

VII. CONCLUSIONS

We have considered a network in which a multi-antenna aided BS and an RIS support multiple IUs and EUs. To facilitate computational tractability while aiming for the maximum possible information and energy throughput, conjugate

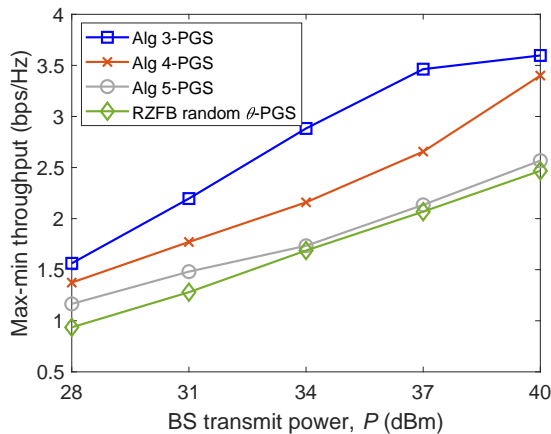


Fig. 8: Achievable minimum throughput for $M = 10$ under RZF vs the BS transmit power P .

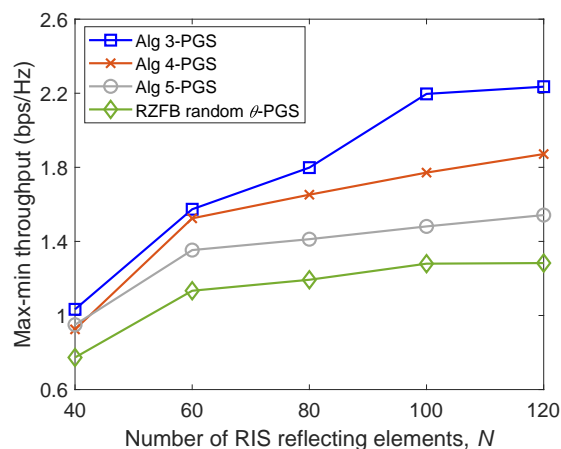


Fig. 9: Achievable minimum throughput for $M = 10$ with energy harvesting under RZF vs RIS for N reflecting elements.

beamforming has been used for delivering energy, while zero-forcing or regularized zero-forcing beamforming has been used for delivering information under the transmit-TS framework, where energy and information are separately delivered during different time-slot fractions. The problem of jointly designing the RIS PRCs and the power allocation of the beamformers for maximizing the minimum IU throughput subject to QoES in terms of the harvested energy thresholds at the EUs end has been addressed. It has been shown that this joint design can be decomposed into separate designs of the RIS PRCs and of the power allocation of the IUs' beamforming. We have developed several efficient algorithms for these designs. A new regularized zero-forcing beamforming method has also been conceived for improving the IUs' throughput, which can improve the IUs' throughput significantly, especially in the regime of low numbers of BS antennas.

APPENDIX: RATE FUNCTION APPROXIMATION

The following inequality follows from the fact that the function $\langle [\mathbf{V}]^2 \mathbf{Y}^{-1} \rangle$ is convex for the the matrix variable \mathbf{V}

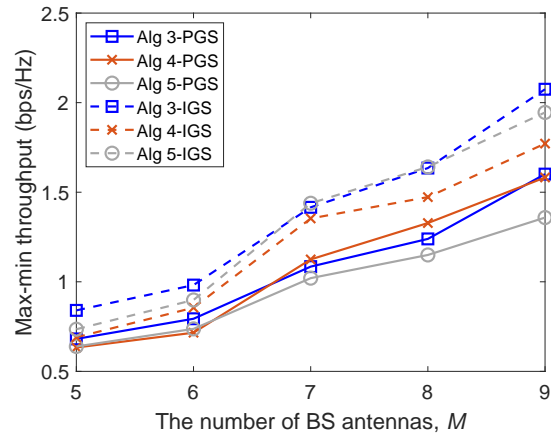


Fig. 10: Achievable minimum throughput under RZF vs the number of BS antennas M .

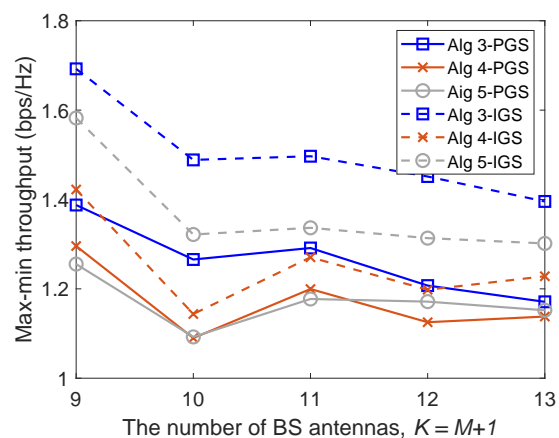


Fig. 11: Achievable minimum throughput under RZF for $K = M + 1$ BS antennas.

and positive matrix variable \mathbf{Y} [35]:

$$\langle [\mathbf{V}]^2 \mathbf{Y}^{-1} \rangle \geq 2\Re\{\langle \bar{\mathbf{V}}^H \bar{\mathbf{Y}}^{-1} \mathbf{V} \rangle - \langle [\bar{\mathbf{V}}]^2 \bar{\mathbf{Y}}^{-1} \mathbf{Y} \bar{\mathbf{Y}}^{-1} \rangle\}, \quad (86)$$

for all \mathbf{V} , $\bar{\mathbf{V}}$, and positive definite \mathbf{Y} and $\bar{\mathbf{Y}}$ of an appropriate dimension.

The following inequalities were obtained in [36]:

$$\ln \left(1 + \frac{\mathbf{v}^2}{\mathbf{y}} \right) \geq \ln \left(1 + \frac{\bar{v}^2}{\bar{y}} \right) - \frac{\bar{v}^2}{\bar{y}} + 2 \frac{\bar{v} \mathbf{v}}{\bar{y}(\bar{y} + \bar{v}^2)}, \quad (87)$$

for all $\mathbf{v} \in \mathbb{R}$, $\mathbf{y} > 0$ and $\bar{v} \in \mathbb{R}$, $\bar{y} > 0$, and

$$\ln |I_2 + [\mathbf{V}]^2 \mathbf{Y}^{-1}| \geq \ln |I_2 + [\bar{\mathbf{V}}]^2 \bar{\mathbf{Y}}^{-1}| - \langle [\bar{\mathbf{V}}]^2 \bar{\mathbf{Y}}^{-1} \rangle - \langle \bar{\mathbf{Y}}^{-1} - ([\bar{\mathbf{V}}]^2 + \bar{\mathbf{Y}})^{-1}, [\mathbf{V}]^2 + \mathbf{Y} \rangle + 2\Re\{\langle \bar{\mathbf{V}}^H \bar{\mathbf{Y}}^{-1} \mathbf{V} \rangle\}, \quad (88)$$

for all matrices \mathbf{V} and $\bar{\mathbf{V}}$, and positive definite matrices \mathbf{Y} and $\bar{\mathbf{Y}}$ of size 2×2 .

Particularly,

$$\ln \left(1 + \frac{\mathbf{v}^2}{\sigma} \right) \geq \ln \left(1 + \frac{\bar{v}^2}{\sigma} \right) - \frac{\bar{v}^2}{\sigma} + 2 \frac{\bar{v} \mathbf{v}}{\sigma}$$

$$\frac{\bar{v}^2 (\sigma + \mathbf{v}^2)}{\sigma(\sigma + \bar{v}^2)} \quad (89)$$

for $\sigma > 0$ and $\mathbf{v} \in \mathbb{R}$, $\bar{v} \in \mathbb{R}$.

REFERENCES

- [1] J. Hu, K. Yang, G. Wen, and L. Hanzo, "Integrated data and energy communication network: A comprehensive survey," *IEEE Commun. Surveys Tuts.*, vol. 20, pp. 3169–3219, Fourthquarter 2018.
- [2] L. Zhao, X. Wang, and K. Zheng, "Downlink hybrid information and energy transfer with massive MIMO," *IEEE Trans. Wirel. Commun.*, vol. 15, pp. 1309–1322, Feb. 2016.
- [3] A. A. Nasir, H. D. Tuan, D. T. Ngo, T. Q. Duong, and H. V. Poor, "Beamforming design for wireless information and power transfer systems: Receive power-splitting versus transmit time-switching," *IEEE Trans. Commun.*, vol. 65, pp. 876–889, Feb. 2017.
- [4] H. H. M. Tam, H. D. Tuan, A. A. Nasir, T. Q. Duong, and H. V. Poor, "MIMO energy harvesting in full-duplex multi-user networks," *IEEE Trans. Wirel. Commun.*, vol. 16, pp. 3282–3297, May 2017.
- [5] H. Yu, H. D. Tuan, T. Q. Duong, Y. Fang, and L. Hanzo, "Improper Gaussian signaling for integrated data and energy networking," *IEEE Trans. Commun.*, vol. 68, pp. 3922–3934, Jun. 2020.
- [6] H. Yu, H. D. Tuan, A. A. Nasir, T. Q. Duong, and L. Hanzo, "Improper Gaussian signaling for computationally tractable energy and information beamforming," *IEEE Trans. Vehic. Techn.*, vol. 69, no. 11, pp. 13990–13995, 2020.
- [7] C. B. Peel, B. M. Hochwald, and A. L. Swindlerhurst, "A vector-perturbation technique for near capacity multiantenna multiuser communication-Part I: channel inversion and regularization," *IEEE Trans. Commun.*, vol. 53, pp. 195–202, Jan. 2005.
- [8] L. D. Nguyen, H. D. Tuan, T. Q. Duong, and H. V. Poor, "Multi-user regularized zero forcing beamforming," *IEEE Trans. Signal Process.*, vol. 67, pp. 2839–2853, Jun. 2019.
- [9] S. Tretyakov, V. Asadchy, and A. Diaz-Rubio, "Chapter 6: Metasurfaces for general control of reflection and transmission," in *World Scientific Handbook of Metamaterials and Plasmonics*, pp. 249–293, 2017.
- [10] C. Huang, A. Zappone, G. C. Alexandropoulos, M. Debbah, and C. Yuen, "Reconfigurable intelligent surfaces for energy efficiency in wireless communication," *IEEE Trans. Wirel. Commun.*, vol. 18, pp. 4157–4170, Aug. 2019.
- [11] Q. Wu and R. Zhang, "Towards smart and reconfigurable environment: Intelligent reflecting surface aided wireless network," *IEEE Commun. Mag.*, pp. 1–7, 2019.
- [12] M. Di Renzo, M. Debbah, D.-T. Phan-Huy, A. Zappone, M.-S. Alouini, C. Yuen, V. Sciancalepore, G. C. Alexandropoulos, J. Hoydis, H. Gacanin, J. de Rosny, A. Bounceu, G. Lerosey, and M. Fink, "Smart radio environments empowered by AI reconfigurable meta-surfaces: An idea whose time has come," *EURASIP J. Wirel. Commun. Network.*, no. 1, p. 129, 2019.
- [13] C. Huang, S. Hu, G. C. Alexandropoulos, A. Zappone, C. Yuen, R. Zhang, M. D. Renzo, and M. Debbah, "Holographic MIMO surfaces for 6G wireless networks: Opportunities, challenges, and trends," *IEEE Wirel. Commun.*, vol. 27, pp. 118–125, Oct. 2020.
- [14] Q.-U.-A. Nadeem, A. Kammoun, A. Chaaban, M. Debbah, and M.-S. Alouini, "Asymptotic max-min SINR analysis of reconfigurable intelligent surface assisted MISO systems," *IEEE Trans. Wirel. Commun.*, vol. 19, pp. 7748–7764, Dec. 2020.
- [15] G. Zhou, C. Pan, H. Ren, K. Wang, W. Xu, and A. Nallanathan, "Intelligent reflecting surface aided multigroup multicast MISO communication systems," *IEEE Trans. Signal Process.*, vol. 68, pp. 3236–3251, 2020.
- [16] C. Pan, H. Ren, K. Wang, W. Xu, M. ElKashlan, A. Nallanathan, and L. Hanzo, "Multicell MIMO communications relying on intelligent reflecting surface," *IEEE Trans. Wirel. Commun.*, vol. 19, pp. 5218–5233, Aug. 2020.
- [17] H. Yu, H. D. Tuan, A. A. Nasir, T. Q. Duong, and H. V. Poor, "Joint design of reconfigurable intelligent surfaces and transmit beamforming under proper and improper Gaussian signaling," *IEEE J. Sel. Areas Commun.*, vol. 38, pp. 2589–2603, Nov. 2020.
- [18] C. Pan, H. Ren, K. Wang, M. ElKashlan, A. Nallanathan, J. Wang, and L. Hanzo, "Intelligent reflecting surface aided mimo broadcasting for simultaneous wireless information and power transfer," *IEEE J. Select. Areas Commun.*, vol. 38, pp. 1719–1734, Aug. 2020.
- [19] Q. Wu and R. Zhang, "Joint active and passive beamforming optimization for intelligent reflecting surface assisted SWIPT under QoS constraints," *IEEE J. Select. Areas Commun.*, vol. 38, pp. 1735–1748, Aug. 2020.
- [20] C. Huang, R. Mo, and C. Yuen, "Reconfigurable intelligent surface assisted multiuser MISO systems exploiting deep reinforcement learning," *IEEE J. Select. Areas Commun.*, vol. 38, no. 8, pp. 1839–1850, 2020.
- [21] C. Huang, Z. Yang, G. C. Alexandropoulos, K. Xiong, L. Wei, C. Yuen, Z. Zhang, and M. Debbah, "Multi-hop ris-empowered terahertz communications: A drl-based hybrid beamforming design," *IEEE J. Select. Areas Commun.*, vol. 39, no. 6, pp. 1663–1677, 2021.
- [22] H. Tuy, *Convex Analysis and Global Optimization (second edition)*. Springer International, 2017.
- [23] H. Yu, H. D. Tuan, E. Dutkiewicz, H. V. Poor, and L. Hanzo, "Maximizing the geometric mean of user-rates to improve rate-fairness: Proper vs. improper gaussian signaling," *IEEE Trans. Wirel. Commun.*, pp. 1–1, 2021.
- [24] L. Wei, C. Huang, G. C. Alexandropoulos, C. Yuen, Z. Zhang, and M. Debbah, "Channel estimation for RIS-empowered multi-user MISO wireless communications," *IEEE Tran. Commun.*, vol. 69, no. 6, pp. 4144–4157, 2021.
- [25] J. Barzilai and J. M. Borwein, "Two-point step size gradient methods," *IMA J. Numerical Analysis*, vol. 8, no. 1, pp. 141–148, 1988.
- [26] P. Apkarian and H. D. Tuan, "Robust control via concave minimization local and global algorithms," in *Proc. of the 37th IEEE Conf. Decision Control*, pp. 3855–3860, 1998.
- [27] P. Apkarian and H. D. Tuan, "Concave programming in control theory," *J. of Glob. Optim.*, vol. 15, pp. 243–270, Apr. 1999.
- [28] P. Apkarian and H. D. Tuan, "Robust control via concave optimization: local and global algorithms," *IEEE Trans. Autom. Control*, vol. 45, pp. 299–305, Feb. 2000.
- [29] K. P. Bennett and O. L. Mangasarian, "Bilinear separation of two sets in n -space," *Computat. Optim. Applicat.*, vol. 2, pp. 207–227, 1993.
- [30] K. Zhou and J. Doyle, *Essentials of Robust Control*. Prentice Hall, 1999.
- [31] R. Schneider, *Convex Bodies: The Brunn-Minkowski Theory*. Cambridge University Press, Cambridge, 1993.
- [32] D. Peaucelle, D. Henrion, and Y. Labit, "Users guide for SeDuMi interface 1.03," 2002.
- [33] P. J. Schrierer and L. L. Scharf, *Statistical Signal Processing of Complex-Valued Data: The Theory of Improper and Noncircular Signals*. Cambridge University Press, 2010.
- [34] T. M. Cover and J. A. Thomas, *Elements of Information Theory (second edition)*. John Wileys & Sons, 2006.
- [35] U. Rashid, H. D. Tuan, H. H. Kha, and H. H. Nguyen, "Joint optimization of source precoding and relay beamforming in wireless MIMO relay networks," *IEEE Trans. Commun.*, vol. 62, pp. 488–499, Feb. 2014.
- [36] H. H. M. Tam, H. D. Tuan, and D. T. Ngo, "Successive convex quadratic programming for quality-of-service management in full-duplex MU-MIMO multicell networks," *IEEE Trans. Commun.*, vol. 64, pp. 2340–2353, Jun. 2016.



Hongwen Yu received the Bachelor and Master degree from Shanghai University, Shanghai, China in 2011 and 2014, respectively, and received Ph.D. degree in Communication and Information Engineering from the Shanghai University, Shanghai, China, in 2020. He is currently pursuing the Ph.D. degree with the School of Electrical and Data Engineering, University of Technology Sydney, Ultimo, NSW, Australia. His current research interests include optimization methods for wireless communication and signal processing.



Hoang Duong Tuan received the Diploma (Hons.) and Ph.D. degrees in applied mathematics from Odessa State University, Ukraine, in 1987 and 1991, respectively. He spent nine academic years in Japan as an Assistant Professor in the Department of Electronic-Mechanical Engineering, Nagoya University, from 1994 to 1999, and then as an Associate Professor in the Department of Electrical and Computer Engineering, Toyota Technological Institute, Nagoya, from 1999 to 2003. He was a Professor with the School of Electrical Engineering and Telecommunications, University of New South Wales, from 2003 to 2011. He is currently a Professor with the School of Electrical and Data Engineering, University of Technology Sydney. He has been involved in research with the areas of optimization, control, signal processing, wireless communication, and biomedical engineering for more than 20 years.

communications, University of New South Wales, from 2003 to 2011. He is currently a Professor with the School of Electrical and Data Engineering, University of Technology Sydney. He has been involved in research with the areas of optimization, control, signal processing, wireless communication, and biomedical engineering for more than 20 years.



Eryk Dutkiewicz received his B.E. degree in Electrical and Electronic Engineering from the University of Adelaide in 1988, his M.Sc. degree in Applied Mathematics from the University of Adelaide in 1992 and his PhD in Telecommunications from the University of Wollongong in 1996. His industry experience includes management of the Wireless Research Laboratory at Motorola in early 2000 's. Prof. Dutkiewicz is currently the Head of School of Electrical and Data Engineering at the University of Technology Sydney, Australia. He is a Senior

Member of IEEE. He also holds a professorial appointment at Hokkaido University in Japan. His current research interests cover 5G/6G and IoT networks.



H. Vincent Poor (S72, M77, SM82, F87) received the Ph.D. degree in EECS from Princeton University in 1977. From 1977 until 1990, he was on the faculty of the University of Illinois at Urbana-Champaign. Since 1990 he has been on the faculty at Princeton, where he is currently the Michael Henry Strater University Professor. During 2006 to 2016, he served as the dean of Princeton's School of Engineering and Applied Science. He has also held visiting appointments at several other universities, including most recently at Berkeley and Cambridge. His research

interests are in the areas of information theory, machine learning and network science, and their applications in wireless networks, energy systems and related fields. Among his publications in these areas is the forthcoming book *Machine Learning and Wireless Communications* (Cambridge University Press). Dr. Poor is a member of the National Academy of Engineering and the National Academy of Sciences and is a foreign member of the Chinese Academy of Sciences, the Royal Society, and other national and international academies. He received the IEEE Alexander Graham Bell Medal in 2017.



Lajos Hanzo (<http://www-mobile.ecs.soton.ac.uk>, https://en.wikipedia.org/wiki/Lajos_Hanzo) (FIEEE'04) received his Master degree and Doctorate in 1976 and 1983, respectively from the Technical University (TU) of Budapest. He was also awarded the Doctor of Sciences (DSc) degree by the University of Southampton (2004) and Honorary Doctorates by the TU of Budapest (2009) and by the University of Edinburgh (2015). He is a Foreign Member of the Hungarian Academy of Sciences and a former Editor-in-Chief of the IEEE

Press. He has served several terms as Governor of both IEEE ComSoc and of VTS. He has published 2000+ contributions at IEEE Xplore, 19 Wiley-IEEE Press books and has helped the fast-track career of 123 PhD students. Over 40 of them are Professors at various stages of their careers in academia and many of them are leading scientists in the wireless industry. He is also a Fellow of the Royal Academy of Engineering (FREng), of the IET and of EURASIP.